ROAD MATERIALS AND PAVEMENT DESIGN
2025, VOL. 26, NO. 9, 2373–2402
https://doi.org/10.1080/14680629.2024.2443234

Statistical investigation of aggregate size and shape impact on porosity and compressive strength of pervious concrete

Mohan Sajeevan, Navakulan Ahilash, Jeyaseelan Shobijan, Varatharaja Pravinjan, Karunanithy Virupashan, Navaratnarajah Sathiparan and Daniel Niruban Subramaniam

Department of Civil Engineering, University of Jaffna, Killinochchi, Sri Lanka

ABSTRACT

The shape and size of aggregates are rarely investigated in pervious concrete research despite their impact on porosity and compressive strength. This study analyses the impact of size and shape distribution of aggregates and mix design on compressive strength and porosity of pervious concrete. 486 specimens of 81 different designs (aggregate-size, aggregate-shape, aggregate-to-cement ratio and compaction) were investigated. Compressive strength was measured after 28 days of curing. The porosity of samples was estimated as theoretical porosity (computed from constituent ratios) and measured porosity (using water displacement). Data visualisation was used for pattern recognition while ANOVA, Post-hoc and Bayesian independent *t*-Tests were employed to statistically verify effects. A significant impact of aggregate-shape on porosity and compressive strength was observed while aggregate size significantly lesser impact. Aggregate to cement ratio had a larger impact on compressive strength while compaction had a significant yet lower impact. Porosity and compressive strengths had different relationships for different shapes of aggregates.

ARTICLE HISTORY
Received 29 April 2024
Accepted 10 December 2024

KEYWORDS
Aggregate size; aggregate shape; pervious concrete; statistical tests; compressive strength

1. Introduction

Pervious concrete is predominantly designed to be applied as a porous paving material in urban catchments that also encompasses other benefits, including noise reduction and heat insulation (Akand et al., 2016; Andrew & Bradley, 2010; Chen et al., 2012; Obla, 2007; Shen et al., 2021; Sonebi & Bassuoni, 2013). Mostly constitutes only coarse aggregates and binder (cement or at time supplementary cementitious materials such as flyash), while occasionally including a small amount (approximately 5%) of fine aggregates (Ahilash et al., 2022; Deo et al., 2010; Reyad et al., 2024; Sandoval et al., 2020; Supriya & Murali, 2023; Tang et al., 2023). The induced pores in the structure significantly reduce the strength while increasing porosity which, in turn, enhances permeability and noise and heat insulation characteristics (Lian & Zhuge, 2010; Pieralisi et al., 2015; Sathiparan et al., 2024b).

Contemporary studies on pervious concrete, mostly found since the late 2010s, have harnessed exponentially increased attention, owing to its potential as a sustainable material. Most studies are based on laboratory experiments while a few studies assessed its application in parking lots and low-traffic roads and pavements (Anburuvel & Subramaniam, 2023a; Bonicelli et al., 2013; Bonicelli et al., 2016; Chandrappa & Biligiri, 2018; Haselbach & Freeman, 2007; Sandoval et al., 2020; Shu et al., 2011). Laboratory-based studies often vary mix design parameters, including water-to-cement ratio, aggregate-to-cement ratio, aggregate size and supplementary binder material (Anburuvel & Subramaniam, 2024; Chandrappa & Biligiri, 2018; Chen et al., 2012; Neithalath et al., 2010; Singh et al., 2019;

CONTACT Daniel Niruban Subramaniam daniel.subramaniam@gmail.com

Zhong & Wille, 2015; Zhu et al., 2023). Although admixtures enhance the strength characteristics of pervious concrete, wider industrial applications may find the cost to be more critical a factor which, in turn, restricts admixture addition (Anburuvel & Subramaniam, 2023b; Sajeevan & Subramaniam, 2023; Sonebi & Bassuoni, 2013).

The two conditions to be satisfied in the process of casting pervious concrete are 1. zero slump and 2. zero compaction, to avoid blocking of the bottom surface due to the migration of binder paste during casting (Subramaniam et al., 2022; Torres et al., 2015; Xie et al., 2018; Xu et al., 2020; Yu et al., 2023). In contrast to the casting of conventional concrete, where the mix is assumed as continuous (as Bingham Plastic) paste and coarse aggregates are woven into the fabric of binder-fine aggregates, pervious concrete is often modelled as an arrangement of binder-coated aggregate particles (Nguyen et al., 2014; Pieralisi et al., 2016; Sathiparan et al., 2024a; Sriravindrarajah et al., 2012; Subramaniam et al., 2022; Subramaniam, Jeyananthan, et al., 2024b). In other words, during the mixing, aggregate particles establish a coating of binder-water paste, which, when cast in the moulds, assumes a skeleton structure of connected binder-coated aggregates. Restriction to the migration of paste further ensures that the structure is unadjusted unlike that in conventional concrete. This process induces in addition, a unique packing of binder-coated aggregates, which contrives high uncertainty in the performance of the resulting pervious concrete (Subramaniam et al., 2022; Wijekoon et al., 2024a). Should compaction be given to the wet mix upon casting, the binder-coated aggregates would be manoeuvered and mobilised to assume more uniform packing, while the same will squeeze the binder paste within the pores, subsequently reducing porosity. Unique packing and hence derived uncertainty in the performance of resulting concrete hinder the wider industrial application of pervious concrete despite its beneficial characteristics for sustainable engineering (Chandrappa & Biligiri, 2018; Huang et al., 2010; Huang et al., 2021; Kovac & Sicakova, 2017). Studies have shown that provision of an optimised amount of compaction energy enhances the uniformity and strength performance of pervious concrete without compromising the permeability and porosity (as intended for subsequent applications) (Anburuvel & Subramaniam, 2022a, 2023b; Sathiparan et al., 2024a; Subramaniam et al., 2022; Wijekoon et al., 2024a).

Supplying compaction energy to the wet mix of pervious concrete, re-arranging binder-coated aggregates, redistributing excess binder-paste in pores, thereby effectively reduces the binder thickness of the coat. The thickness of the binder being sandwiched between aggregates and significantly reduced, it increases the contact surface area between aggregates. The distribution of binder-paste around the surface of the aggregates is often modelled on the assumption that the aggregate particles are spherical and are of the same diameter in a particular mix. However, it is comprehensible that aggregate particles are neither of the same size nor spherical. The distribution of binder-coating around aggregate particles is predominantly affected by the size and shape distribution of aggregate particles (Sajeevan et al., 2023; Subramaniam, Sajeevan, et al., 2024; Wijekoon et al., 2023). For example, a model could assume that irrespective of the sizes of aggregates, all binder-coated aggregates would be of the same diameter (small aggregates having thicker coating and larger aggregates having thinner coating) while another model could assume that all aggregates, irrespective of their sizes, would result in equal thickness of coating (Huang et al., 2021; Jato-Espino et al., 2014; Nguyen et al., 2014; Pieralisi et al., 2015, 2016). In reality, the actual binder thickness may be between the two models discussed above. In addition, it could be assumed that irrespective of the shape of an aggregate, the binder may coat it in equal thickness, while another model could be assumed to have binder coating of higher thickness at the angular edges than flat surfaces of the aggregate (Akand et al., 2016; Huang et al., 2021; Wang et al., 2020; Wen et al., 2020). It is understandable that the size and shape distribution of aggregates will have a significant impact on the binder-coating around aggregate particles.

As such, when compaction energy is applied and distributed in the wet mix of pervious concrete, the rearrangement of particles will result in further distortions in the binder-coat thickness distribution along and between aggregate particles. The wet mix being not a continuous media (as opposed to conventional concrete), the distribution of compaction energy would be even more affected by

Table 1. Mechanical properties of aggregates.

Properties	Value
Bulk density (kg/m^3)	1491
Specific gravity	2.72
Absorption (%)	0.20
Moisture content (%)	0.35
Aggregate Impact value – AIV (%)	25.5
Aggregate Crushing Value – ACV (%)	30.5
Flakiness Index	14.7
Elongation Index (%)	24.02

the size and shape distribution of aggregate particles (Awed et al., 2015; Bonicelli et al., 2013; Kirkham & Whiffin, 1951; Kokubu et al., 1996). In turn, the heterogeneous distribution of compaction energy, along the lateral and vertical profile of pervious concrete wet mix, would further distort the binder-coating of aggregates and filling of pores (Mueller et al., 2014; Pietzsch & Poppy, 1992; Zhang et al., 2016). It is, therefore, understandable that the impact of aggregate size and shape on the effective optimisation of other mix design parameters, including constituent ratios and compaction, is vital in developing more uniform characteristics of pervious concrete for industrial applications. This study is designed as a laboratory-scale controlled experiment to apprehend the impact of aggregate size and shape distribution on the performance of pervious concrete, specifically on the porosity and compressive strength. The objective of the study also includes the assessment of how the impact of shape and size distribution of aggregates on porosity and compressive strength is affected by aggregate-to-cement ratio and compaction.

2. Methodology

This section provides information on the experiments and data analyses carried out in order in this research study. Experiments are divided into two phases. Aggregate tests were carried out in Phase 01 which is also the preparation of aggregates for Phase 02. Phase 02 contains tests on prepared pervious concrete specimens with different mix designs including differently shaped aggregates.

2.1. Materials

Primary material gneiss-derived crushed aggregates were obtained from local suppliers. Ordinary Portland cement was used as binder material which is obtained from a local vendor. Water was obtained from the tap in the Department of Civil Engineering, University of Jaffna supplied by the water board, Sri Lanka. Then, aggregates were tested in the laboratory, as summarised in Table 1. The results indicate that aggregates satisfy the required quality to be used as coarse aggregate in pervious concrete sample preparation.

In Phase 02 of the experiments, aggregates had to be prepared for concrete casting. As the impact of shape and size distribution of aggregate in pervious concrete is a major objective of the study, the aggregates should be classified according to size and shape. The aggregates were milled in the Los Angeles Abrasion Value (LAAV) instrument to obtain the required shape variation. While one class of aggregates was not milled, the other two classes of aggregates were milled in the LAAV instrument for 200 and 1000 revolutions. 200 and 1000 revolutions were selected from a previous study, which observed a significant change in the surface morphology of aggregates with 200 and 1000 revolutions (Subramaniam, Dassanayake, et al., 2024a; Wijekoon et al., 2023). Milled aggregates were washed and dried to remove dust particles. The aggregates were then sieved and separated into 5–12 mm, 12–18 mm and 18–25 mm classes to assess the impact of aggregate size on the performance of pervious concrete.

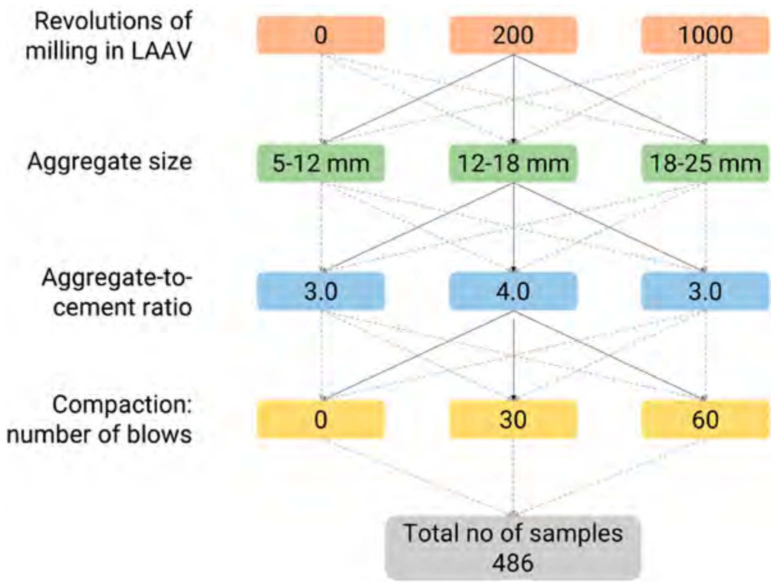

Figure 1. Summary of the specimen mix-design details.

2.2. Pervious concrete specimen casting

Figure 1 shows the details of the mix-design parameters, their values and the mix-designs. Water-to-cement ratio was maintained at 0.3 to ensure the slump is zero to avoid segregation of the binder from the mix (Sathiparan et al., 2024a; Wijekoon et al., 2024b). A total of 81 mix designs were adopted in this study, in each mix design, six samples were prepared and altogether 486 samples were prepared.

Twenty-minute mixing protocol was adopted for the preparation of the fresh concrete, as illustrated in Figure 2. The fresh concrete was checked for zero slump and then 150 mm × 150 mm × 150 mm cube samples were prepared. The mould was filled by three equal layers and the compaction energy was also equally distributed for each layer. After 24 h of drying at room temperature cube samples were demoulded and cured in water for 28 days.

2.3. Specimen performance testing

The performance test for samples was carried out for all six samples and all the other tests should be completed before testing the compressive strength as it is a destructive test.

2.3.1. Porosity

The study is carried out for two types of porosity measurements. Type one is calculated from the mix proportions of the design and the wet weight of the concrete cube. Using the density and proportions volume of each component in the cube can be calculated. When subtracting each component volume from the cube volume, it provides the volume of the pore. When dividing the pore volume by total volume, porosity can be obtained theoretically and it is called T.Poro in the study.

Type two is determined using the dry weight of the sample and the submerged weight of the sample in water. The difference between the dry sample and the submerged weight of the sample provides the weight of the replaced water by the solid part of the sample. The volume of replaced water is equal to the solid content of the cube and it could be reduced from the total volume of the cube to get the pore volume. When the pore volume is divided by total volume or by directly using Equation (1)

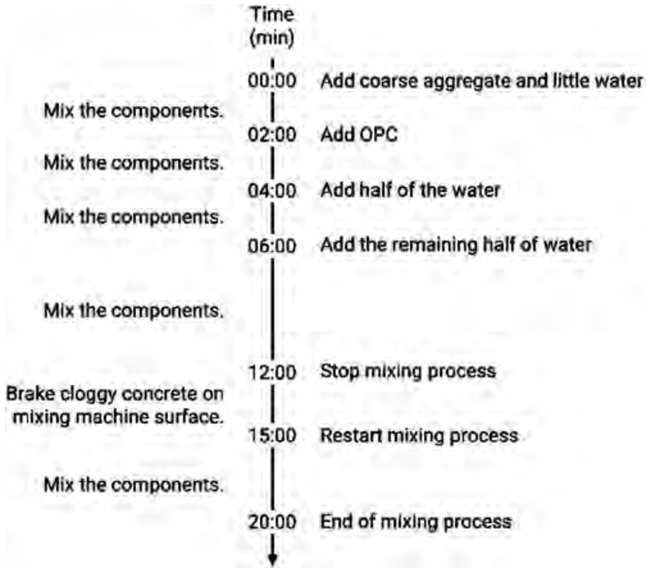

Figure 2. Flow diagram of mixing protocol for pervious concrete casting.

measured porosity (M.Poro) can be determined.

$$v = \left[1 - \frac{w_d - w_w}{\rho_w V}\right] \tag{1}$$

where v is the total void ratio; w_d is the weight of oven-dried sample (kg); w_w is the weight of sample in water (kg); ρ_w is the density of water (kg/m^3); V is the volume of sample (m^3).

2.3.2. Compressive strength

The compressive strength of the sample cube was tested using a universal testing machine (UTM). The load was applied by displacement control at a 1-mm/min rate. The specimens were taken from the water tank after 28 days of curing and let to dry at room temperature. Then, the compressive strength of pervious concrete was determined based on BS1881: Part 116: 1983.

2.4. Data analysis

The obtained data were transferred to an Excel spread sheet and organised with respective mix designs. Further analysis was carried out using Microsoft Excel, SPSS and JM Pro software.

2.4.1. Data visualisation and descriptive statistics

To learn the basics of the obtained data, a scatter plot was used between Theoretical Porosity, Measured Porosity, Compressive strength, size of aggregates and shape of aggregates. Meanwhile, to address the relationship between parameters in the plots, curve fitting was done for linear function and gradient, cut-off value and R^2 value were compared. After obtaining the fundamental learning from data using data visualisation and descriptive statistics, further advanced statistical techniques were applied.

2.4.2. Distribution analyses

Distribution analyses are the deep analysis beyond the data visualisation and descriptive statistics to understand the data critically with the distribution. The analysis focuses on the shape and the pattern of the spread of data.

In this study, histogram and box plots are used in distribution analysis visualisation and mean, standard deviation, skewness and kurtosis are used in distribution analysis descriptive statistics.

Histogram	Bar chart with the number of bins of the data and indicates the frequency in each bin. The distribution of the data could be observed clearly.
Boxplot	Summarise the data with a box for the median and with whiskers for the spread of the data. Multiple box plots can be plotted in one graph to compare.

2.4.2.1. Skewness. Skewness describes the asymmetry of the distribution function. If the skewness value is zero, the distribution is normally distributed. A positive value describes that the distribution is skewed to the right and a negative value describes that the distribution is skewed to the left.

$$\text{Skewness} = \frac{\sum_{i}^{n} (x_i - \bar{x})^3}{n\sigma^3}$$

x_i is every data points in the dataset; $\bar{x}$ is the mean value; n is the number of data points; σ is the standard deviation.

2.4.2.2. Kurtosis. Kurtosis contains the information on how the data are concentrated near the mean value. If the kurtosis is zero, the distribution is normally distributed. A positive value describes that the data are concentrated near the mean value and a negative value describes that the data are scattered around the mean value.

$$\text{Kurtosis} = \frac{\sum_{i}^{n} (x_i - \bar{x})^4}{n\sigma^4} - 3$$

x_i is the data point in the dataset; $\bar{x}$ is the mean value; n is the number of data points; σ is the standard deviation.

Initially, the distribution analyses were carried out for the whole dataset for theoretical porosity, measured porosity and compressive strength. Then dataset was sorted with shape, compaction, aggregate-to-cement ratio and aggregate size and analysed separately to observe the behaviour of dependent parameters.

2.4.3. Analysis of variance (ANOVA) test

One way analysis of variance (ANOVA) is an advanced statistical method used to compare the means of groups to identify whether they have a statistically significant difference between them. In the ANOVA test, initially, a null hypothesis was created as all the groups of data are the same and an alternative hypothesis was created as at least one pair of groups is not equal. Then, the variance between the means of a group from the overall mean and the variance inside the group from the mean of the group was calculated. Then the variance was divided by the degree of freedom and the mean square of variance will be calculated for both variances separately.

$$\text{Mean of Variation} = \frac{\text{Sum of Variation}}{\text{Degree of Freedom}}$$

F value is calculated using both mean variations as shown in Equation X.

$$F\ \text{value} = \frac{\text{Mean variation between group}}{\text{Mean variation within group}}$$

By considering the calculated F value as the F Critical value and using the F statistic table, the P value will be obtained. P value will be used to interpret the significance of the ANOVA test.

2.4.3.1. Post-HOC test – LSD. Post HOC tests are conducted on data to explore the summarise results received in ANOVA in detail. These tests are adopted to identify which specific groups are significantly different between them by pair-wise analysis. The least significance test (LSD) is the post HOC test used after ANOVA test analysis in this study to understand the significant difference between pairs of groups.

2.4.4. Bayesian independent t-test

The Bayesian independent *t*-test is a statistical test used to compare the means of two independent groups when information about prior beliefs about the parameters is available. Unlike the traditional frequentist *t*-test, it incorporates prior knowledge through Bayesian inference to provide richer and more nuanced information about the difference between the means. Instead of *p*-values (probability of observing the data under the null hypothesis), the Bayesian approach focuses on posterior probabilities representing the updated belief about the difference in means after considering both the data and the prior information. Bayesian independent *t*-test was adopted to confirm the findings of one-way ANOVA test and Post-HOC–LSD tests carried out in this study.

3. Results and discussion

3.1. Data visualisation and descriptive statistics

Measure Porosity (M.Poro) and Theoretical Porosity (T.Poro) were computed based on two different methods of assessing the porosity of pervious concrete specimens. The methods of quantifying porosities in two methods are discussed in the methodology. The variation of M.Poro against T.Poro is shown in Figure 3 for different aggregate-shaped specimens. The difference in M.Poro between milled and unmilled specimens was distinctive as observed in the figure, where it was higher for unmilled specimens. As higher degree of milling enhances spherecity in aggregate morphology, yielded progressively lower M.Poro for milled specimens compared to unmilled specimens with comparable T.Poro. The observation of discrepancy corresponds to higher theoretical porosity, although the percentage is comparable for higher and lower theoretical porosities. The numerical models that represent the trend (best fitting linear regression model) establish that the unmilled specimens had $y = x + c$ (the gradient m is almost close to 1) where c is approximately −0.05. This is interpreted as M.Poro is approximately 0.05 less than T.Poro for all porosities (all specimens). This could be explained as almost a fraction of pores are inaccessible and not accounted for in M.Poro, they were accounted for in T.Poro. The percentage of pores of T.Poro that were not accessible varies with the T.Poro. For example, a difference of 0.05 in a T.Poro of 0.1 will be 50% while a difference of 0.05 in a T.Poro of 0.3 would be 16.7%.

A similar observation of $y = x + c$ could also be done for T.Poro-M.Poro relationship for 200 Rev specimens, yet the constant ‘c’ is now −0.14. This observation indicates that more pores become inaccessible when aggregates become smoother in texture. In other words, 0.15 porosity being inaccessible in a T.Poro of 0.3 would now be approximately 50%, compared to 16.7% in the unmilled specimens. On further investigation of the figure, it could be established that the accuracy of the model is highly compromised for 200 Rev specimens (R^2 of 0.73) compared to 0.94 from the unmilled specimens. A lower accuracy in the model indicates a higher uncertainty in the relationship in milled specimens, which could be attributed to the change in aggregate morphology (considering all other parameters being kept constant between experiments). Although a linear model still best describes the overall trend for T.Poro–M. Poro relationship for extensively milled (1000 Rev) specimens, the gradient of the linear plot is now reduced to 0.5 instead of 1 observed for 0 and 200 Rev specimens. The constant ‘c’ becomes −0.19, when the model was retrofitted to a gradient of 1 ($y = x + c$) with an R^2 of 0.52 (further increased uncertainty). It could be concluded that the aggregate shape significantly influences pore connectivity for comparable total porosity values.

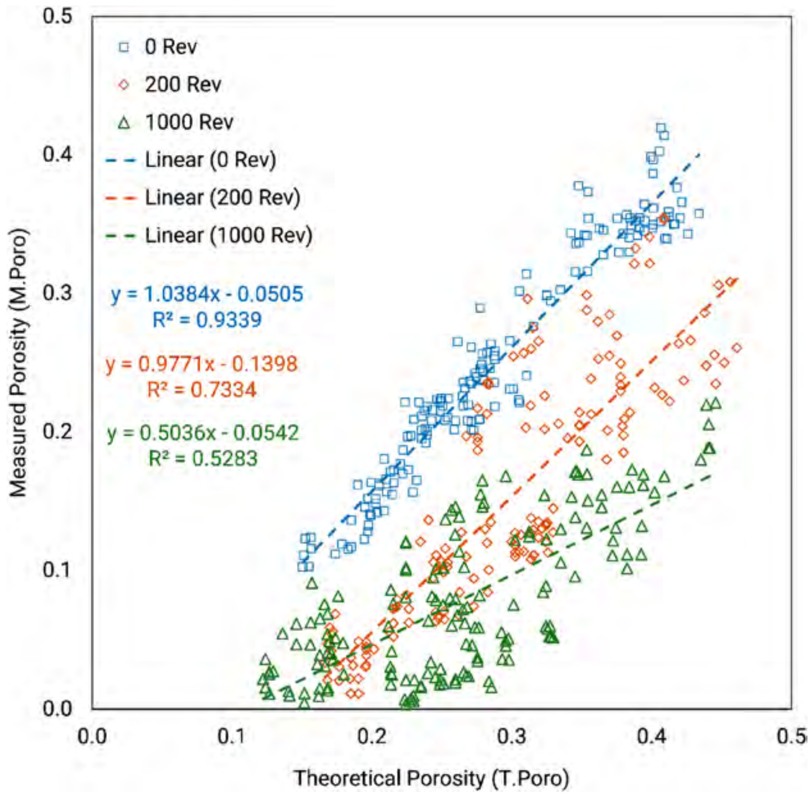

Figure 3. Variation of measured porosity with theoretical porosity for different aggregate shapes.

Figure 4 illustrates the variation of compressive strength with (a) theoretical porosity and (b) measured porosity of pervious concrete for different aggregate shapes. A significant difference could be observed between the models for T.Poro and M.Poro. As shown in Figure 4(a), linear models exhibit lower accuracy for unmilled specimens (0.46) while the same enhances to 0.84 and 0.71 for 200 and 1000 Rev specimens. This indicates that the predictability of compressive strength from T.Poro significantly improved for milled specimens (and remained rather consistent between 200 and 1000 revolutions). The uncertainty in the model or unmilled specimens was much higher, indicating a higher non-linear impact of other design parameters on compressive strength. Simultaneously, a lower uncertainty in 200 and 1000 Rev specimens indicates a more uniform and linear impact of other parameters on compressive strength. Considering the gradient of linear models, a rapid increment is observed from −65.44 to −100.37 between unmilled and 200 Rev specimens and only an increment to −107.3 for 1000 Rev specimens. Furthermore, a rapid increment could also be observed for 'c' from 29.042 to 46.07 for unmilled and 200 Rev specimens, while it increased only to 48.405 for 1000 Rev specimens. This indicates a rapid change in the variation from 0 to 200 Rev of aggregate shape change, while a larger increment in revolutions yielded much lower performance enhancement.

Considering Figure 4(b), the trend for M.Poro is significantly different from T.Poro. For example, an increase from 0.545 to 0.736 was observed in accuracy (R^2) for 0 and 200 Rev while an even more significant loss to 0.289 was observed for 1000 Rev. While the uncertainty in the model is quite low for 200 Rev, the uncertainty in 1000 Rev specimens is more random than any trend indicated. The spread around the linear best-fitting curve for 1000 Rev reinstates that the model could not be used for any prediction. Further looking at the gradient values of −66.19, −82.44 and −98.63 for 0, 200

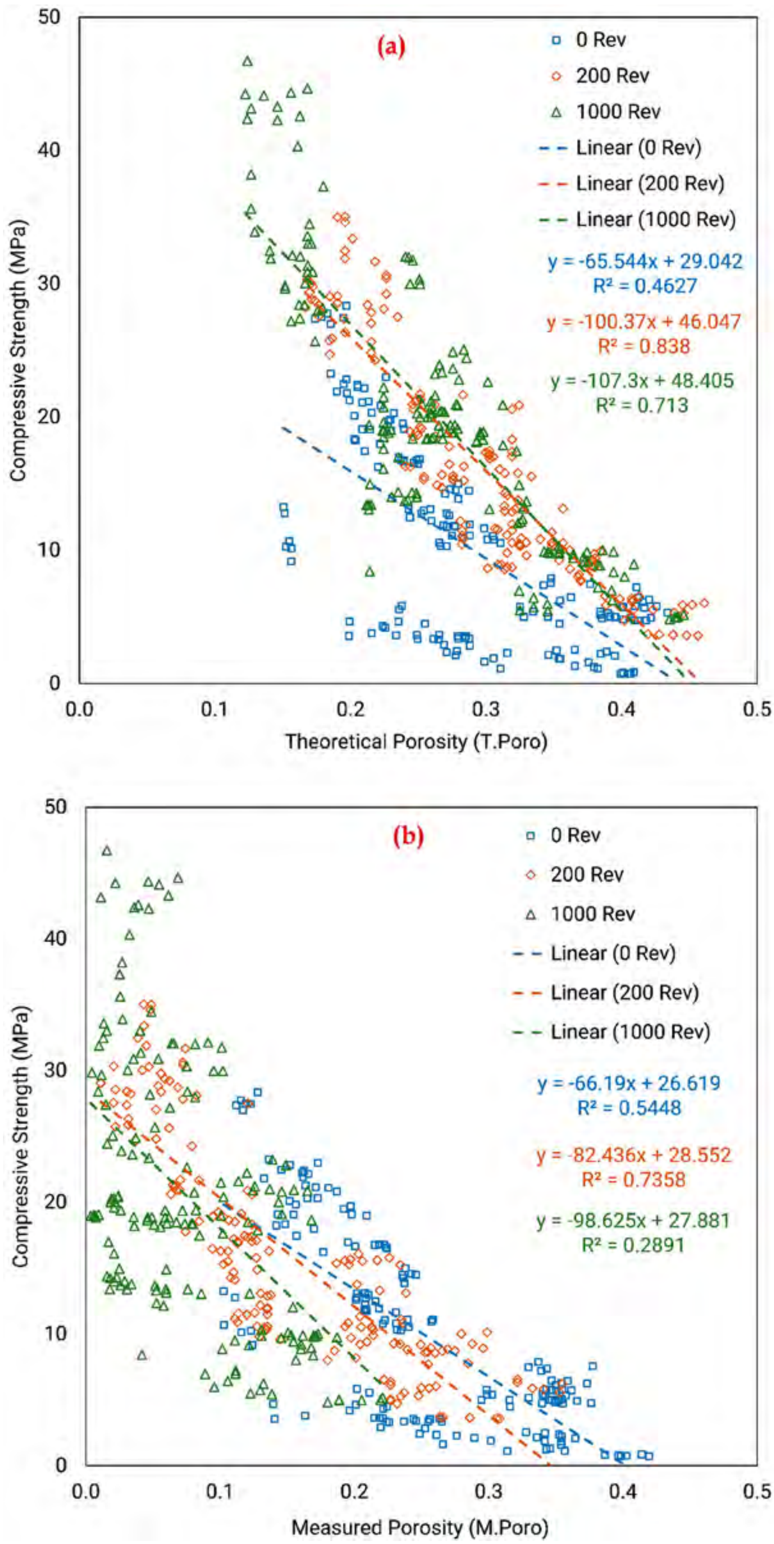

Figure 4. Variation of compressive strength for different shape aggregates with (a) theoretical porosity and (b) measured porosity.

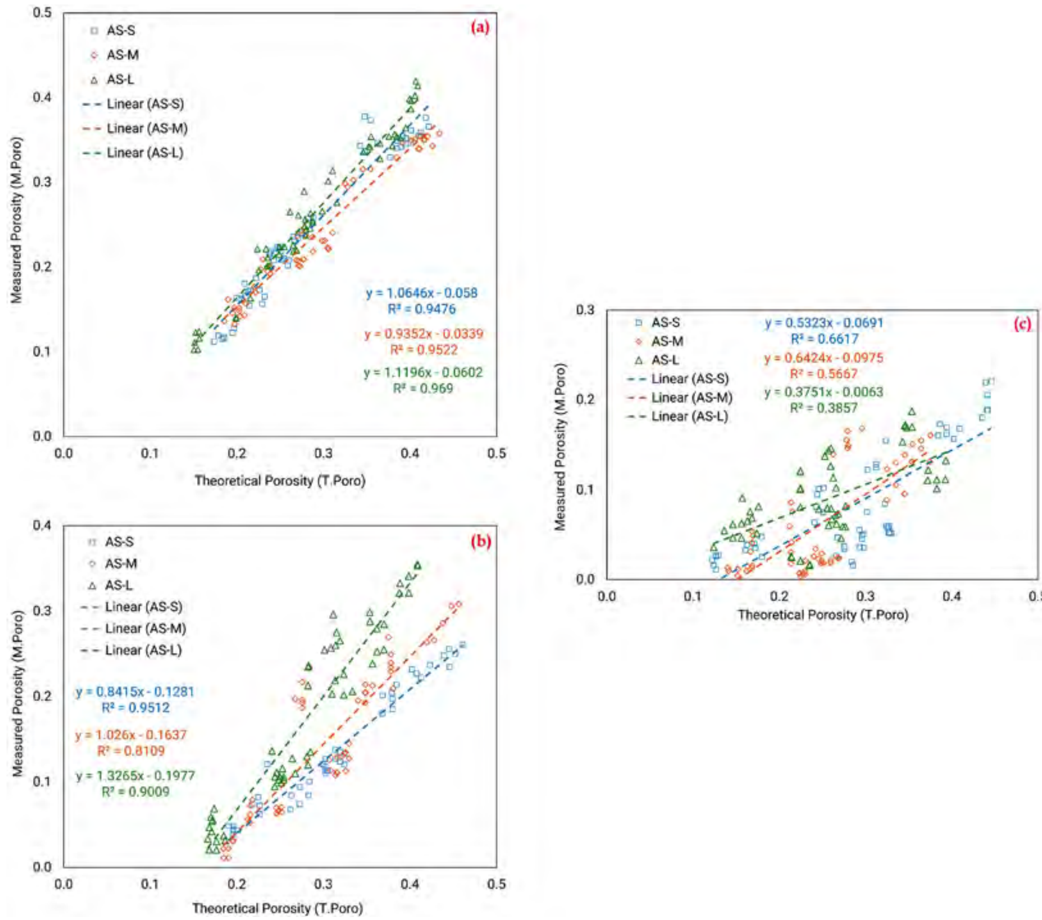

Figure 5. Variation of M.Poro with T.Poro for (a) 0 Rev, (b) 200 Rev and (c) 1000 Rev, for different aggregate sizes.

and 1000 Rev, a decreasing increment could be observed between 0–200 and 200–1000 Rev. Simultaneously, 'c' values of 26.62, 28.55 and 28.91 for 0, 200 and 1000 Rev specimens, respectively indicate rather consistent values across three different aggregate shapes. A significant improvement observed for T.Poro in 'c' values is not evident for M.Poro. The observations indicate that the impact of both T.Poro and M.Poro on compressive strength are neither similar nor of any correspondence. It further indicates that the impact T.Poro and M.Poro has on compressive strength is significantly and non-uniformly affected by other design parameters.

The impact of aggregate shape (Rev) on the relationship between aggregate size (AS) and compressive strength (Com.S) indicated by individual plots (for Rev) is shown in Figure 5. All linear models of AS-Com.S relationship pertaining to 0 Rev aggregates have almost perfect representation, indicated by R^2 values of 0.95, 0.95 and 0.97 for AS-S (5–12 mm), AS-M (12–18 mm) and AS-L (18–25 mm), respectively. Low uncertainty indicates that for unmilled aggregates, the compressive strength varies linearly with T.Poro, irrespective of the size of aggregates used. Models have gradients of 1.06, 0.93 and 1.12 for AS-S, AS-M and AS-L indicate that it is rather consistent for all aggregate sizes. In addition, constant 'c' values of −0.058, −0.033 and −0.060 for AS-S, AS-M and AS-L, respectively, further reinstate that the linear models for AS-S, AS-M and AS-L are rather consistent across aggregate sizes, for unmilled specimens. In other words, a linear representation may be used to represent M.Porosity-T.Porosity relationship for all aggregate sizes, collectively, with a small compromise on accuracy (R^2 of 0.92).

Table 2. Descriptive statistics summary of the entire data matrix.

	Descriptive statistics							
	N	Min	Max	Mean	Std.Dev	Var	Skew	Kurtosis
T.Poro	486	0.12	0.46	0.2844	0.07971	0.006	0.16	−0.8
M.Poro	486	0	0.42	0.1604	0.10689	0.011	0.368	−0.844
Com.S	486	0.72	46.72	15.363	9.68736	93.845	0.744	0.15

For 200 Rev specimens (Figure 5(b)), a significant deviation between the linear representation could be observed between aggregate sizes. The accuracy of the linear models was 0.91, 0.85 and 0.90 for AS-S, AS-M and AS-L, respectively, which was significantly lower than those of 0 Rev specimens, but a strong representation of the trend. The gradients of the linear models were 0.842, 1.026 and 1.327 for AS-S, AS-M and AS-L, which are significantly different, indicating a significant deviation of the model from a collective representation. The constant 'c' was 0.13, 0.16 and 0.20 for AS-S, AS-M and AS-L, which is also significantly different. In other words, for 200 Rev specimens, the relationship between T.Poro and M.Poro varies significantly for different aggregate sizes.

Figure 5(c) shows the plots for 1000 Rev specimens, where the linear model accuracy could be observed to drop to 0.66, 0.57 and 0.39 for AS-S, AS-M and AS-L, respectively. The model is rather random for large aggregate specimens of 1000 Rev while high uncertainty with a general linear trend could be seen for both small- and medium-size aggregate specimens. The gradient and constant 'c' are quite consistent between small- and medium-size aggregate specimens of 1000 Rev. However, the gradient and constant 'c' vary rather randomly, and owing to randomness in the model fit, as discussed above.

3.2. Distribution analyses

Analyses on the distribution of values pertaining to each parameter would be beneficial in assessing the impact of aggregate shape on the compressive strength of pervious concrete specimens. Table 2 gives the descriptive summary of the entire experimental data used in the study. The mean of T.Poro, M.Poro and Com.S of all 486 specimens was 0.2844, 0.1604 and 15.353, respectively, while the corresponding standard deviation was 0.0797, 0.1689 and 9.687. The standard deviation for both M.Poro and Com.S was almost 50% of the corresponding mean while it was 25% for T.Poro. The observation establishes a larger impact of the independent parameters on the performance parameters (M.Poro, T.Poro and Com.S). The frequency distribution (histogram) of the respective performance parameters is shown in Figure 6. The figure indicates a normal distribution fitted for T.Poro, which is supported by very low skew values (from Table 2: 0.16). However, the distribution of M.Poro and Com.S has a heavy skew of 0.368 and 0.744, respectively. As discussed earlier, for unmilled (0 Rev) specimens, irrespective of other design parameters, T.Por and M.Poro were linearly correlated with a statistical significance of 0.92 (R^2) and, therefore, would essentially assume the same shape. Simultaneously, Com.S being heavily dependent on porosity, the distribution would also assume the same distribution shape. In milled aggregates, M.Poro and T.Poro have no significant correlation, the shapes of the distribution of performance parameters would be essentially different. M.Poro is essentially in the shape of an exponential distribution pattern, while Com.S is in the shape of lognormal or Weibull functions. Kurtosis describes how sharp a curve is at the peak of the distribution curve. The observations show that Kurtosis of all three performance parameters is significantly different, indicating different trends induced by wider types of impact of the design parameters. Figure 7 highlights the difference between the probability distribution function reinforced for T.Poro and M.Poro. The skew of M.Poro to the left is apparent compared to an almost symmetric distribution (potentially attributed to a normal distribution pattern) that could be observed for T.Poro.

Analysis of the impact of each independent parameter on the distribution of performance parameters is discussed in this section. Weibull probability distribution function (PDF) of M.Poro, T.Poro and

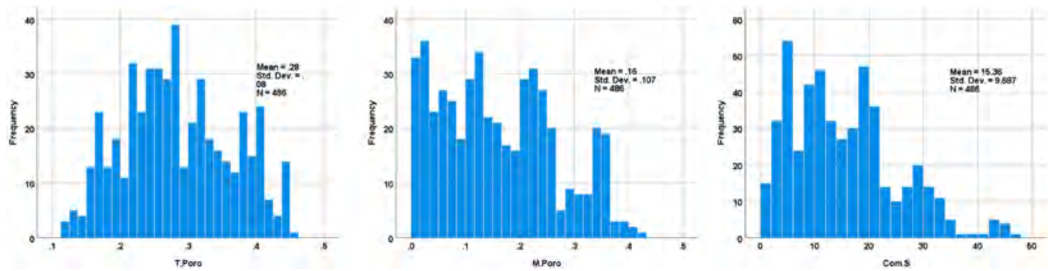

Figure 6. Histogram representation of T.Poro, M.Poro and Com.S for all 486 samples.

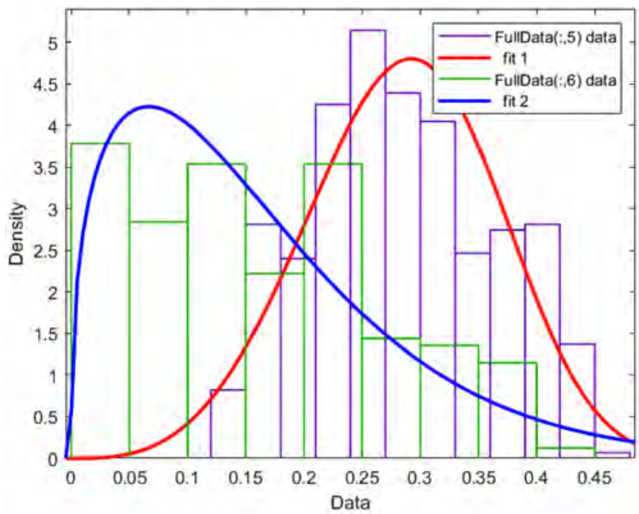

Figure 7. Weibull distribution fit for T.Poro (Red) and M.Poro (Blue) for 486 samples.

Com.S for 0, 200 and 1000 Rev sample classes is shown in Figure 8. PDF of T.Poro was close in profile to a symmetric distribution which is also consistent across three classes of aggregate shape-based specimens. The other three design parameters (AC, compaction and AS) contribute to the distribution of T.Poro. Skew of T.Poro (Figure 9) of T.Poro was 0.257, 0.073 and 0.248 for 0, 200 and 1000 Rev, respectively. A skew close to 0 indicates a normal distribution, which is observed for 200 Rev, while a significant skew is observed for both 0 and 1000 Rev. Kurtosis for 0, 200 and 1000 Rev was −1.081, −0.817 and −0.580, respectively, which indicates a progression of increment in the sharpness of the peak of T.Poro with a number of revolutions (Rev). The negative kurtosis indicates a wider distribution; however, the absolute values less than 3.0 imply the absence of outliers. These two observations collectively indicate the minimal or insignificant impact of Rev on T.Poro.

On the other hand, a significant shift of mean towards lower value is observed for M.Poro, progressively skewing towards the same with Rev (Figure 8). In contrast to that of T.Poro, distribution of M.Poro was close to normal distribution for 0 Rev, which then skewed heavily in 200 and 1000 Rev. While a Weibull PDF could be approximated for 200 Rev, an exponential PDF best describes the distribution of 1000 Rev. The skew was 0.158, 0.305 and 0.584 and the kurtosis is −1.111, −0.984 and −0.766 for 0, 200 and 1000 Rev, respectively. This shows that the peaks are sharper with increased Rev cthan the observations made in T.Poro. In addition, the outliers are not significant for M.Poro as well, indicating a significant impact of aggregate shape on M.Poro.

In contrast to the observations above, the distribution of Com.S for 0 Rev reveals a significantly skewed distribution compared to the same in 200 and 1000 Rev (Figure 8). The skew of Com.S is more

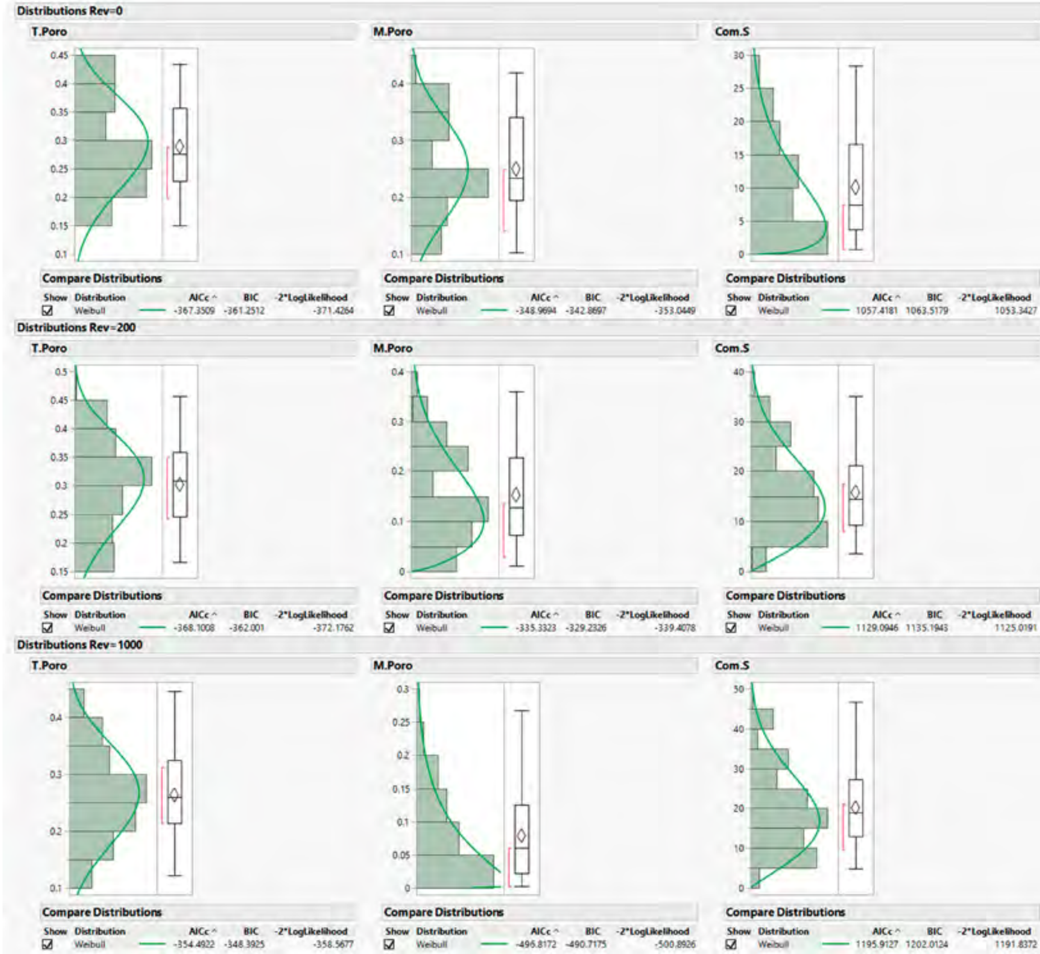

Figure 8. Distribution of T.Poro, M.Poro and Com.S for 0, 200 and 1000 Rev sample classes (162 samples in each group).

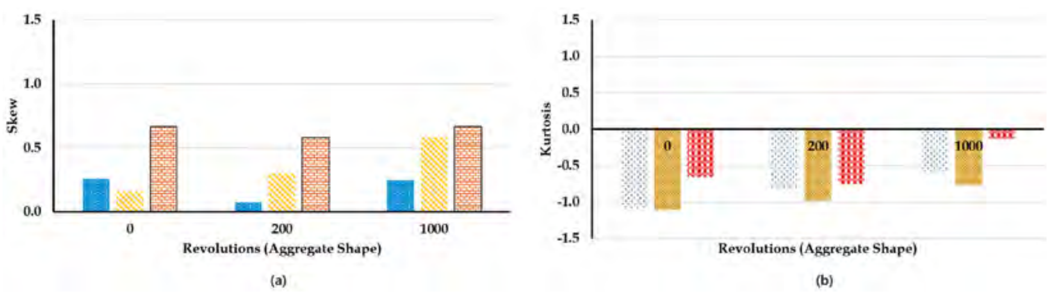

Figure 9. Distribution of (a) skew and (b) Kurtosis for 0, 200 and 1000 Rev sample classes (162 samples in each group).

towards a lower strength for 0 Rev than that observed in 200 and 1000 Rev. The symmetricity of the distribution enhances with Rev indicated by skew values of 0.668, 0.581 and 0.467 for 0, 200 and 1000 Rev, respectively (Figure 9). Kurtosis was −0.657, −0.755 and −0.127 which reinstates the absence of outliers and that the shape of the distribution significantly changes for 1000 Rev. The impact of aggregate

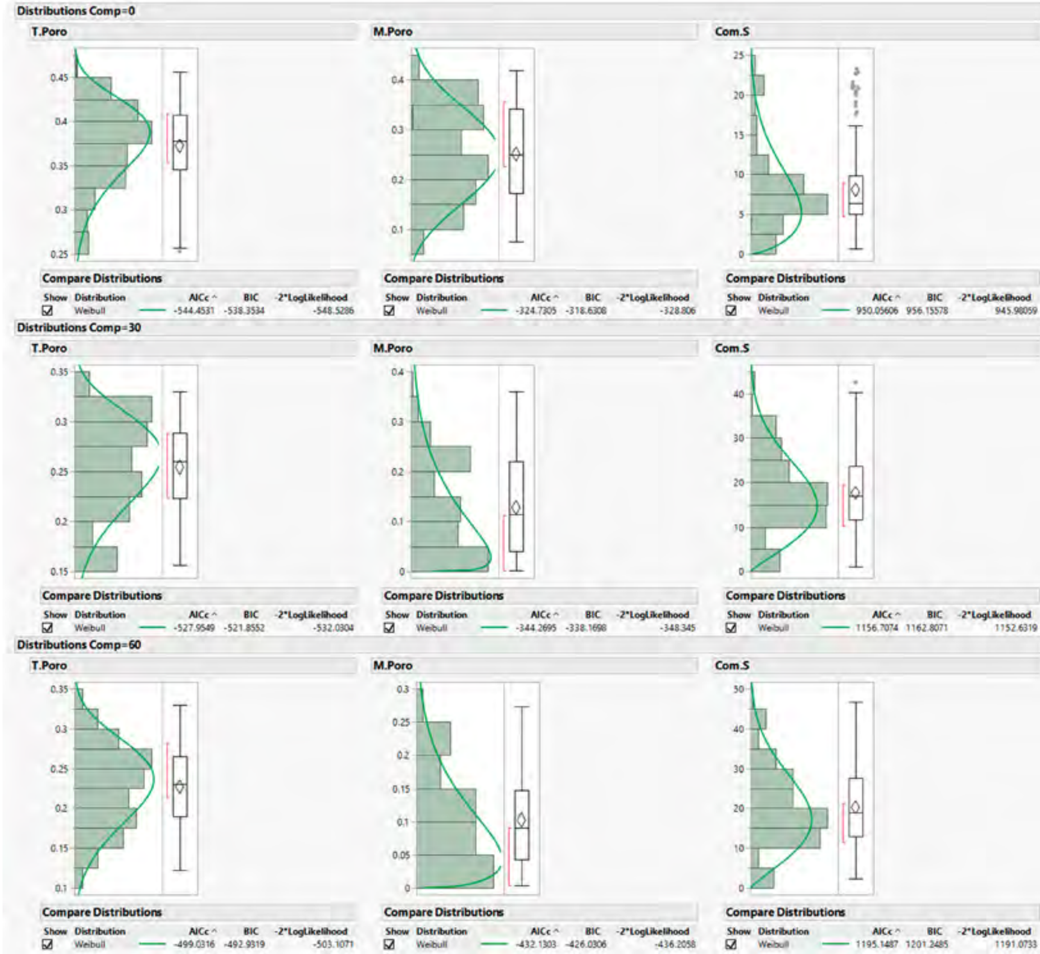

Figure 10. Distribution of T.Poro, M.Poro and Com.S for 0, 30 and 60 blows of compaction sample classes (162 samples in each group).

shape is significant, specifically between milled and unmilled samples, while the more rounded the aggregates are, more gain in compressive strength could be deduced from these initial observations.

Figures 10 and 11 show histograms, Weibull PDF fit, variation of skew and kurtosis for T.Poro, M.Poro and Com.S for samples with 0, 30 and 60 blows of compaction. Similar to observations made in the previous analysis, the distribution of T.Poro remains consistent and close to a normal distribution for all compactions, indicating a rather insignificant impact on the distribution shape. However, a significant shift in mean values from approximately 0.375–0.4, 0.25–0.275 and 0.225–0.25 for 0, 30 and 60 blows could be observed. Comparatively less drop between 30 and 60 blows of compaction indicates an impact of compaction which is more in the lower range on T.Poro where 30 blows of compaction were optimum in previous studies too (Anburuvel & Subramaniam, 2022a; Subramaniam et al., 2022). While a normal distribution could be observed for M.Poro for 0 blows, a significantly skewed profile could be observed for both 30 and 60 blows. Similar to observations made with T.Poro, a significant (much steeper drop) could be observed in mean values, indicated by 0.25–0.275, 0.05–0.075 and 0.025–0.05 for 0, 30 and 60 blows of compaction. Similar to the impact of revolutions, a skewed shape of the distribution of Com.S for 0 compaction samples was close to normal distribution for 30 and 60 blows of compaction. Mean values close to 5 MPa were observed for uncompacted samples (0 blows) while

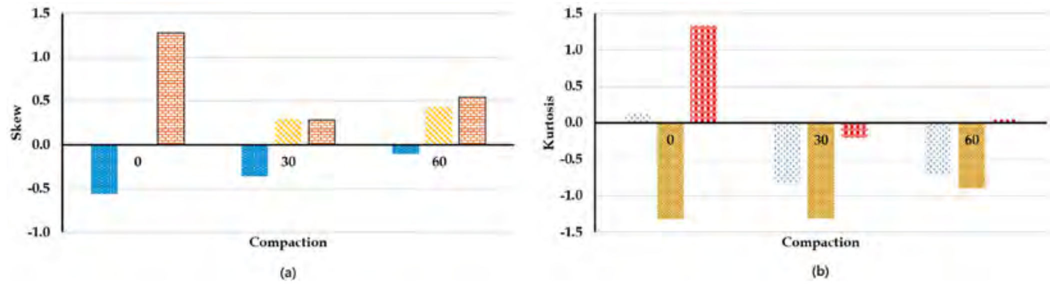

Figure 11. Distribution of (a) skew and (b) Kurtosis for 0, 30 and 60 blows of compaction sample classes (162 samples in each group).

the mean was enhanced to 15 and 20 MPa for 30 and 60 blows of compaction, respectively. These observations confirm that compaction significantly enhances the compressive strength of pervious concrete, while the optimum level of compaction is approximately 30 blows.

Investigation on skew and kurtosis plots from Figure 11 indicates that a similar progressive change was observed in skew for T.Poro (from negative values) and M.Poro (positive values), indicating a significant impact of compaction on the distribution of the same. A significant difference could be observed in skew for Com.S between uncompacted and compacted samples, while a slight difference could also be observed between 30 and 60 blows of compaction. A significant change between compacted and uncompacted specimens could be observed on T.Poro and Com.S when kurtosis is considered, while no significant change is observed between specimen classes for M.Poro, as shown in Figure 11. The analysis of the distribution shows a significant impact from compaction on all three parameters, contriving changes in different aspects of the distribution profile, while the conclusions from previous studies, where an optimum level of compaction of 30 blows, is also observed to be highlighted in this analysis.

Figures 12 and 13 show the distribution of frequencies, Weibull fit, skew and kurtosis of T.Poro, M.Poro and Com.S of samples with aggregate to cement (AC) ratios of 3–5. Similar to observations made from the impact of compaction on the performance variables, the AC ratio also does not significantly affect the shape of the distribution of T.Poro, indicated by a rather symmetric normal distribution profile for all classes. The mean values of T.Poro increase were indicated by 0.25, 0.325 and 0.35 for 3–5 AC ratios. An increment in the AC ratio induces more pores due to a lack of binder content, which is reflected in this observation. Similar to the optimum value for compaction, the same studies have shown that an optimum AC ratio could be 0.35–0.4 for pervious concrete, which is also observed by large increment in the mean between 3 and 4 (0.25–0.325) and comparatively smaller increment between 4 and 5 (0.325–0.35) in this distribution analysis. M.Poro shows a significantly skewed profile for all three classes of AC ratio specimens while the mean changes from 0.05 to 0.1 between 3 and 4 AC ratios. While the increment is significantly less for M.Poro that that of T.Poro, no significant change is observed in M.Poro mean between 4 and 5 AC ratio specimens. This could imply that other parameters affect the impact of the AC ratio on M.Poro.

While a rather insignificant impact was observed on the skew for T.Poro and Com.S (Figure 13), a significant drop in the skew is observed between 3 AC ratio specimens and both 4 and 5 ratio specimens. The same observation could also be made on the values shown for kurtosis, where the values are rather consistent for T.Poro and Com.S for all AC ratios, while a significant drop was observed between 3 and other classes for M.Poro.

Figures 14 and 15 show the distribution of frequency profile, Weibull fit, skew and kurtosis of T.Poro, M.Poro and Com.S of aggregates of mean sizes 8.5, 15 and 21.5 mm classes. Similar trends were observed for T.Poro with almost symmetrical normal distribution. In contrast, the mean was consistent for all aggregate sizes. This may be construed as that the impact of aggregate size on T.Poro may not be significant. Considering the profile of M.Poro it could be observed that all profiles reveal

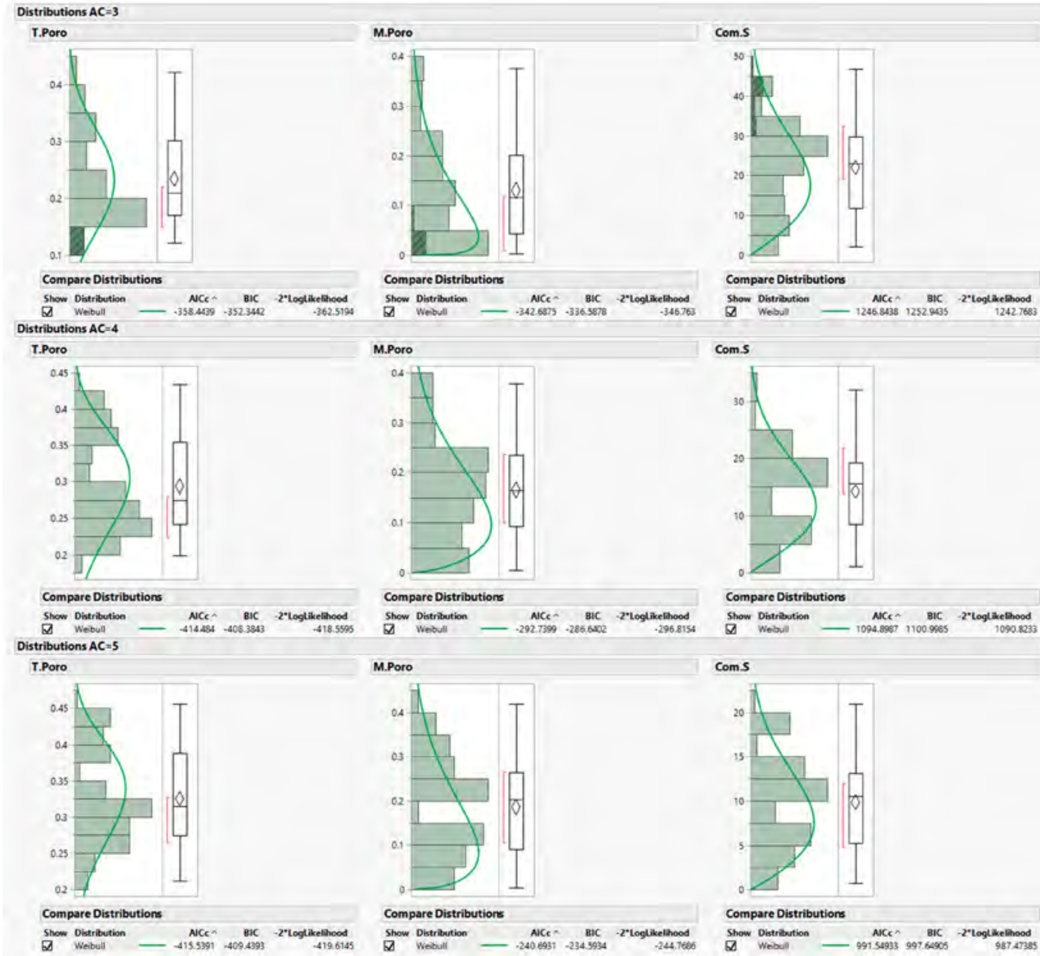

Figure 12. Distribution of T.Poro, M.Poro and Com.S for 3–5 aggregate-to-cement (AC) ratio sample classes (162 samples in each group).

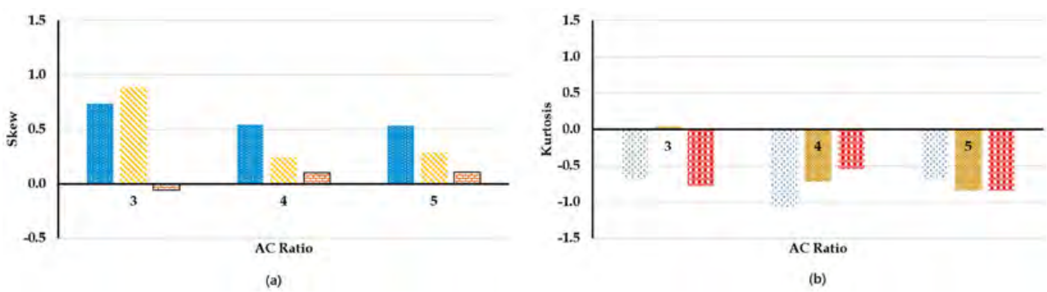

Figure 13. Distribution of (a) skew and (b) Kurtosis for 3–5 aggregate-to-cement (AC) ratio sample classes (162 samples in each group).

a skew to the lower values, similar to T.Poro, the mean value remains rather consistent between 0.05 and 0.1 for all aggregate classes. However, a slight decrease in M.Poro could be observed (congruent to more skew) for medium size aggregates (15 mm) compared to the other two, which have similar trends and mean values. This may indicate that the packing of the binder-coated aggregates for the

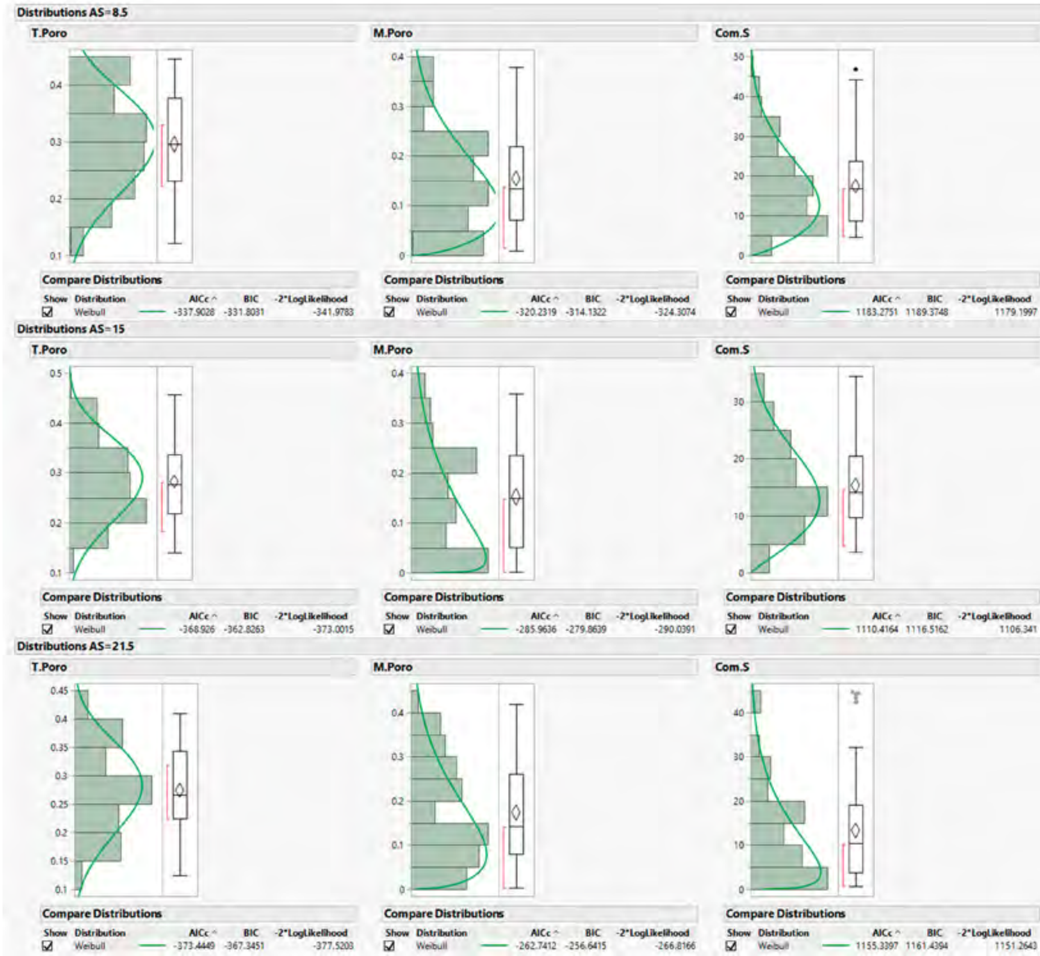

Figure 14. Distribution of T.Poro, M.Poro and Com.S for 8.5, 15 and 21.5 mm mean-aggregate size sample classes (162 samples in each group).

AC ratios considered is more optimum in packing, specifically with the shapes and compaction considered to contribute significantly. While the distribution profile and mean values (10–15 MPa) of Com.S remain constant between aggregates of 8.5 and 15 mm, a significant change in the profile indicated by a skew towards lower values with a mean (approximately 5 MPa) was observed. The larger aggregates could, therefore, be attributed to less strength, perhaps due to the packing of binder-coated aggregates affected by compaction, AC ratio and compaction.

In contrast to changes observed between different classes for T.Poro and M.Poro on skew and kurtosis, a significant change could be observed between larger and other (small and medium) aggregates. The impact of aggregate size will have to be investigated to better optimise the mix-design.

3.3. One-way ANOVA test and analyses

Distribution analyses discussed above have highlighted the significant impact of independent parameters; however, further statistical analyses are required to define the impact with statistical significance. This section discusses one-way ANOVA conducted on the data matrix. Since one-way ANOVA can only applied to univariate data, applying the test essentially assumes that the impact of the testing

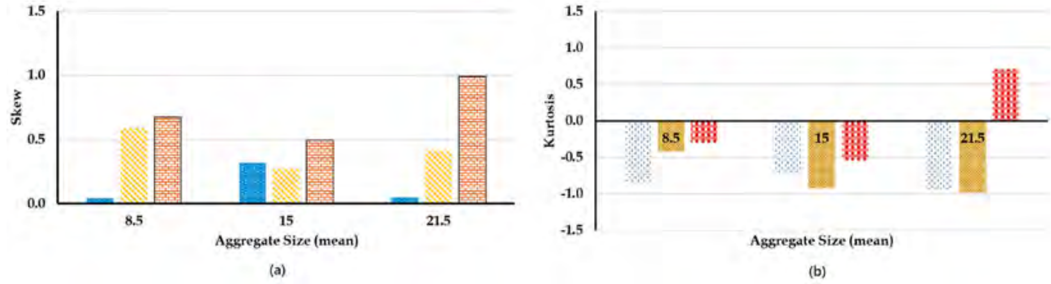

Figure 15. Distribution of (a) skew and (b) Kurtosis for 38.5, 15 and 21.5 mm mean-aggregate size sample classes (162 samples in each group).

Table 3. Results of one-way ANOVA conducted on the data matrix to understand the impact of revolutions (Rev).

		Sum of squares	df	Mean square	F	Sig.
T.Poro	Between groups	0.12	2	0.06	9.765	0
	Within groups	2.962	483	0.006		
	Total	3.082	485			
M.Poro	Between groups	2.379	2	1.19	181.692	0
	Within groups	3.162	483	0.007		
	Total	5.541	485			
Com.S	Between groups	8229.931	2	4114.965	53.307	0
	Within groups	37284.855	483	77.194		
	Total	45514.786	485			

Table 4. One-way ANOVA conducted on the data matrix to understand the impact of compaction (Comp).

		Sum of squares	df	Mean square	F	Sig.
T.Poro	Between groups	1.933	2	0.967	406.453	0
	Within groups	1.149	483	0.002		
	Total	3.082	485			
M.Poro	Between groups	2.061	2	1.03	142.966	0
	Within groups	3.481	483	0.007		
	Total	5.541	485			
Com.S	Between groups	13419.061	2	6709.531	100.97	0
	Within groups	32095.725	483	66.451		
	Total	45514.786	485			

parameter on the performance (dependent) parameter is uniform and linear across other parameters. Tables 3–6 show the output of one-way ANOVA conducted on the data matrix to understand the impact of revolutions (Rev), compaction (Comp), aggregate-to-cement ratio (AC) and aggregate size (AS), respectively. There is a significant difference (95% confidence) between groups on all performance parameters (T.Poro, M.Poro and Com.S) except for one case (Table 6). The case where no significant difference was observed was on M.Poro for the impact of aggregate sizes.

According to the computational equation of *F* value, a higher *F* value would indicate a larger variation between sample means for variation within samples. Considering the *F* values of T.Poro and M.Poro Table 3 show 9.765 and 181.692, respectively. While both quantities measure similar properties (porosity), on a similar scale, the F value of M.Poro is approximately 20 times the *F* value of T.Poro. Considering the mean-square values reported, the mean-square value between groups for M.Poro is 1.19 while it was only 0.06 for T.Poro. The 20 times larger value for M.Poro within groups resulted in a 20 times larger *F* value although the mean-square value for both within groups is comparable (0.006 and 0.007). It could be concluded that the impact of revolutions on M.Poro is highly significant compared

Table 5. One-way ANOVA conducted on the data matrix to understand the impact of aggregate-to-cement ratio (AC).

		Sum of squares	df	Mean square	F	Sig.
T.Poro	Between groups	0.692	2	0.346	69.882	0
	Within groups	2.39	483	0.005		
	Total	3.082	485			
M.Poro	Between groups	0.248	2	0.124	11.336	0
	Within groups	5.293	483	0.011		
	Total	5.541	485			
Com.S	Between groups	12377.407	2	6188.704	90.205	0
	Within groups	33137.379	483	68.607		
	Total	45514.786	485			

Table 6. One-way ANOVA conducted on the data matrix to understand the impact of aggregate size (AS).

		Sum of squares	df	Mean square	F	Sig.
T.Poro	Between groups	0.039	2	0.02	3.099	0.046
	Within groups	3.043	483	0.006		
	Total	3.082	485			
M.Poro	Between groups	0.043	2	0.022	1.905	0.15
	Within groups	5.498	483	0.011		
	Total	5.541	485			
Com.S	Between groups	1397.44	2	698.72	7.65	0.001
	Within groups	44117.346	483	91.34		
	Total	45514.786	485			

to that on T.Poro. A significant difference between the groups is also observed for Com.S (larger variation than T.Poro, but less than in M.Poro), indicating a significantly high impact of aggregate shape on the compressive strength.

A significant difference (95% confidence) is observed between groups for all three parameters based on compaction (Comp), as shown in Table 4. A closer look at the *F* value shows a much larger impact of compaction on T.Poro, indicated by a value of 406.453. The impact of compaction on T.Poro could be considered higher than that of revolution on the same (indicated by an *F* value of 9.765, almost 40 times). Furthermore, the *F* value of M.Poro (142.966) in Table 4 is comparable to that in Table 3 (181.692). This shows that compaction has a comparable impact on M.Poro to that of aggregate shape. The *F* value of Com.S in Table 4 (100.97) is approximately double that in Table 3 (53.307), indicating the impact of compaction is twice higher than that of aggregate shape. The comparative scales discussed here are confined to the range of each variable used and perhaps may relate to either a wider difference between all groups, or a significantly sharp difference between particular groups and comparable between the others. This will be discussed later, with the post-hoc tests, which analyse the difference between each classified group.

F values shown in Table 5 for T.Poro (69.882) are substantially higher than those in Table 3 (9.765) yet, are much significantly lower than those shown in Table 4 (406.453). This indicates that the impact of the AC ratio on T.Poro is more than that of aggregate shape (7 times) but less than that of compaction (approximately 1/7 times). In the meantime, the F value of M.Poro in Table 5 (11.336) is much lesser (1/12 times) in Table 3 (181.692) and Table 4 (142.966). The impact of the AC ratio on M.Poro is, therefore, much less pronounced than compaction and aggregate shape.

Considering *F* values in Table 6, T.Poro, M.Poro and Com.S have 3.099, 1.905 and 7.65, respectively. It has already been established that the aggregate size has no significant impact on M.Poro (confidence is much less than 95%, indicated by Sig of 0.15, shaded in green). The *F* value further confirms that the impact is merely random, and cannot be attributed to the variation in aggregate size. While the impact of aggregate size in T.Poro and Com.S is significant (95% confidence), the impact is rather much less pronounced compared to the impact of compaction, aggregate shape and aggregate-to-cement ratio. For example, AS impacts 1/3 of that of aggregate shape on T.Poro and 1/6 of that of aggregate shape

Table 7. Post-hoc test (LSD) for impact of revolutions (Rev) on the data matrix.

Dependent variable		(I) Rev	(J) Rev	Mean difference (I-J)	Std. error	Sig.
T.Poro	LSD	0	200	−0.0121	0.0087	0.165
			1000	.02556*	0.0087	0.003
		200	0	0.0121	0.0087	0.165
			1000	.03766*	0.0087	0
		1000	0	−.02556*	0.0087	0.003
			200	−.03766*	0.0087	0
M.Poro	LSD	0	200	.09654*	0.00899	0
			1000	.17090*	0.00899	0
		200	0	−.09654*	0.00899	0
			1000	.07436*	0.00899	0
		1000	0	−.17090*	0.00899	0
			200	−.07436*	0.00899	0
Com.S	LSD	0	200	−5.72957*	0.97623	0
			1000	−10.04685*	0.97623	0
		200	0	5.72957*	0.97623	0
			1000	−4.31728*	0.97623	0
		1000	0	10.04685*	0.97623	0
			200	4.31728*	0.97623	0

*The mean difference is significant at the 0.05 level.

on Com.S, indicated by the *F* values. The details of the impact need to be analysed for each group as this could be due to a significant difference between particular groups, and not across all groups.

Looking at the detailed analysis of ANOVA (Post-Hoc) would further help understand the impact of each independent parameter on the performance parameters. Tables 7–10 show the output of Pos-Hoc tests carried out on the ANOVA test described above. On a general inspection, iseveral combinations have been identified not to have significant differences (marked in green). For example, although the ANOVA test in Table 3 revealed that there is a significant difference among groups for T.Poro based on revolutions (Rev). Table 7 shows that there is no significant difference between 0 Rev and 200 Rev samples, indicated by a Sig of 0.165. Rather lower *F* value compared to others as discussed earlier was the result of this combination, while there is a significant difference observed between 200 Rev–1000 Rev and 0 Rev–1000 Rev specimens for T.Poro. A reduction of (by means) approximately 0.02556 (2.5%) and 0.03766 (3.8%) was observed between 0–1000 Rev and 200–1000 Rev, respectively. The lower reduction observed between 0 to 1000 Rev is due to the increase in porosity between 0 Rev and 200 Rev (which is not significant).

Significant differences are observed between all groups for M.Poro and Com.S, indicated by a Sig less than 0.05 (5%). A much higher reduction in M.Poro 0.09654 (9.6%), 0.17090 (17.1%) and 0.07436 (7.4%) was observed between 0–200, 0–1000 and 200–1000 Rev samples. This indicates a larger impact of aggregate shape on the measured porosity (M.Poro), which is progressive (the reduction is comparable between 0–200 and 200–1000 Rev). Compressive strength increased (by means) by 5.72957, 10.04685 and 4.31728 MPa between 0–200, 0–1000 and 200–1000 Rev samples, indicating a consistent increment resulting due to the shape of the aggregate instigated by the process of milling in LAAV.

The output displayed in Table 8 shows a significant difference between all groups for all performance parameters, indicating a significant impact of compaction on all. A mean difference of 0.11825 (11.8%), 0.14522 (14.5%) and 0.02698 (2.7%) of porosity between 0–30, 0–60 and 30–60 blows of compaction, for T.Poro. This is significantly higher compared to the difference induced by the change in aggregate shape, discussed above, which resulted in a 40 times higher F value discussed further above. Simultaneously, a mean difference of 0.12340 (12.3%), 0.14922 (14.9%) and 0.02582 (2.5%) was observed for 0–30, 0–60 and 30–60 blows of compaction. These differences are compared to those observed from the impact of aggregate shape on M.Poro, which resulted in comparable *F* values discussed earlier. The mean difference of 9.56179, 12.24278 and 2.68099 MPa for Com.S for 0–30, 0–60

Table 8. Post-hoc test (LSD) for the impact of compaction (Comp) on the data matrix.

Dependent variable		(I) Comp	(J) Comp	Mean difference (I-J)	Std. error	Sig.
T.Poro	LSD	0	30	.11825*	0.00542	0
			60	.14522*	0.00542	0
		30	0	−.11825*	0.00542	0
			60	.02698*	0.00542	0
		60	0	−.14522*	0.00542	0
			30	−.02698*	0.00542	0
M.Poro	LSD	0	30	.12340*	0.00943	0
			60	.14922*	0.00943	0
		30	0	−.12340*	0.00943	0
			60	.02582*	0.00943	0.006
		60	0	−.14922*	0.00943	0
			30	−.02582*	0.00943	0.006
Com.S	LSD	0	30	−9.56179*	0.90575	0
			60	−12.24278*	0.90575	0
		30	0	9.56179*	0.90575	0
			60	−2.68099*	0.90575	0.003
		60	0	12.24278*	0.90575	0
			30	2.68099*	0.90575	0.003

*The mean difference is significant at the 0.05 level.

Table 9. Post-hoc test (LSD) for impact of aggregate to cement ratio (AC) on the data matrix.

Dependent variable		(I) AC	(J) AC	Mean difference (I-J)	Std. error	Sig.
T.Poro	LSD	3	4	−.05921*	0.00782	0
			5	−.09104*	0.00782	0
		4	3	.05921*	0.00782	0
			5	−.03183*	0.00782	0
		5	3	.09104*	0.00782	0
			4	.03183*	0.00782	0
M.Poro	LSD	3	4	−.03542*	0.01163	0.002
			5	−.05458*	0.01163	0
		4	3	.03542*	0.01163	0.002
			5	−0.01916	0.01163	0.1
		5	3	.05458*	0.01163	0
			4	0.01916	0.01163	0.1
Com.S	LSD	3	4	7.82648*	0.92033	0
			5	12.19969*	0.92033	0
		4	3	−7.82648*	0.92033	0
			5	4.37321*	0.92033	0
		5	3	−12.19969*	0.92033	0
			4	−4.37321*	0.92033	0

*The mean difference is significant at the 0.05 level.

and 30–60 blows of compaction reported indicates a significant impact of compaction on compressive strength. T.Poro, M.Poro and Com.S have shown a much larger impact between 0and 30 compared to that between 30and 60 blows of compaction. This further reinforces the saturation of the impact occurring concerning both these parameters at an optimum compaction of 30 blows, which was also reported in other studies and observed in the distribution analysis earlier.

The mean difference of T.Poro indicates an increase of 0.05921 (5.9%), 0.09104 (9.1%) and 0.03183 (3.2%) between 3–4, 3–5 and 4–5 of AC ratios while it was 0.03542 (3.5%), 0.05458 (5.5%) and 0.01916 (1.9%) for the same ranges for M.Poro, as shown in Table 9. The impact AC ratio has on T.Poro is greater than (almost twice) that on M.Poro. The impact AC ratios have on the porosity in general is less (more than half) than compaction and aggregate shape. In addition, the differences in the mean for both T.Poro and M.Poro is more than double the value between 3 and 4 ratios than that observed between 4 and 5 ratios. This indicates that the impact of the AC ratio subsides or saturates with the

Table 10. Post-hoc test (LSD) for the impact of aggregate size (AS) on the data matrix.

Dependent variable		(I) AS	(J) AS	Mean difference (I-J)	Std. error	Sig.
T.Poro	LSD	8.5	15	0.01385	0.00882	0.117
			21.5	.02168*	0.00882	0.014
		15	8.5	−0.01385	0.00882	0.117
			21.5	0.00783	0.00882	0.375
		21.5	8.5	−.02168*	0.00882	0.014
			15	−0.00783	0.00882	0.375
M.Poro	LSD	8.5	15	0.00264	0.01185	0.824
			21.5	−0.01859	0.01185	0.118
		15	8.5	−0.00264	0.01185	0.824
			21.5	−0.02123	0.01185	0.074
		21.5	8.5	0.01859	0.01185	0.118
			15	0.02123	0.01185	0.074
Com.S	LSD	8.5	15	2.12556*	1.06191	0.046
			21.5	4.15321*	1.06191	0
		15	8.5	−2.12556*	1.06191	0.046
			21.5	2.02765	1.06191	0.057
		21.5	8.5	−4.15321*	1.06191	0
			15	−2.02765	1.06191	0.057

*The mean difference is significant at the 0.05 level.

increment in AC ratios, most likely the optimum impact occurring around 4.0, as observed in previous studies. The mean difference of Com.S of 7.83, 12.20 and 4.37 was observed between 3–4, 3–5 and 4–5 AC ratios. The mean differences observed between groups based on revolutions are less compared to those observed here, indicating AC ratio has a higher impact, which is also comparable to that observed by compaction. However, a sharp drop in the mean difference is observed between 0–30 blows and 30–60 blows of compaction while the drop is more gradual between 3–4 and 4–5 AC ratios. This indicates that the saturation rate in AC impact on compressive strength is more gradual than that was observed by compaction. This is because of the continued decrement in binder material due to increased AC ratios, which continue to increase porosity. On the other hand, compaction can pack binder-coated aggregates to an optimum level and cannot be optimised further, indicating saturation.

Table 10 shows the mixed impact of aggregate size on T.Poro, M.Poro and Com.S as was indicated and discussed in distribution analyses. The one-way ANOVA indicated no significant difference on M.Poro as shown in this table, where no significant difference is observed between any of the combinations. In contrast, while there is no significant difference between 8.5–15 mm and 15–21.5 mm aggregate combination for T.Poro, a significant difference is observed between 8.5 and 21.5 mm aggregate combination. The mean difference is 0.02168 (2.2%) decrement, which indicates that the impact is much less compared to the impact imparted by other independent parameters. From theory, should the particles be mono-size and spherical, their packing arrangement would assume a similar structure, which will result in the same packing density (porosity), irrespective of their sizes. Simultaneously, the sizes of pores would significantly change. However, for heterogeneous aggregate sizes, and aggregates of different shapes, the packing density would not be the same. In this study, the aggregate particles are within a 7–8 mm difference within a group, which could be considered uniform size distribution, yet, the shape of aggregates can be heterogeneously distributed. The results show, that the porosity is rather consistent within the groups, indicating similar packing being assumed irrespective of aggregate sizes. The difference between the 8.5 mm and 21.5 mm aggregate groups observed could be due to the packing being affected by the shape of aggregates.

A much higher significant difference in Com.S is observed between the smallest (8.5 mm) and the largest (21.5 mm) samples indicated by a value of 4.15 MPa. Although a significant difference is observed between the 8.5–15 mm combination, the significance is rather marginal (95.4% confidence) while no significant difference is observed between 15 and 21.5 mm, which again lost the significance marginally (94.7%). Considering the mean differences of 2.13 and 2.03 MPa for 8.5 – 15 mm and 15–21.5 mm, respectively, the difference is almost equal. The variation of values within the group resulted in the significance being accepted and rejected for the respective combinations. Considering the mean differences, if could be observed that the little, but significant impact aggregate size has on the compressive strength is almost consistent with the size (not saturating).

However, the mean differences are subjected to the range of each independent variable considered in this study, in other words, should there not be a saturation on the impact of a variable, a wider range may induce larger differences in the mean. This section analysed if the trends are saturating or progressing for the range of independent variables used in the study. The impact of each independent parameter on the performance parameters is discussed as an overview, and not objectively concluding.

3.4. Bayesian independent t-test

ANOVA test is conducted to anlayse the differences of variances between more than two groups and report significant differences should at least one combination exhibit significant differences. A post-hoc test compliments ANOVA by analysing each pair and adjusting significant values, which was discussed in the previous section. An Independent *t*-Test is carried out to analyse if there is a significant difference between two groups of samples, considering the variances within the group. Both these methods are based on the frequentist approach, which analyses the samples based on hypothetical repeated sampling from the population. These methods have limited uncertainty representation and do not directly account for prior knowledge or beliefs about the effect size.

A Bayesian approach utilises Bayesian statistics, where prior knowledge or beliefs about the effect size are incorporated into the analysis. In addition, instead of *p*-value (significance value), the Bayesian approach generates a posterior distribution, which represents the probability of the true difference between means given the observed data and the prior information. The posterior distribution provides a richer picture of the effect size and its uncertainty, which makes it more interpretable. Furthermore, the prior can be tailored to specific contexts and research questions that reflect existing knowledge or expert opinions.

All observations made from ANOVA and post-hoc tests (significance of differences between combination of sample groups) are confirmed in the Bayesian Independent *t*-Test with high significance indicated by Bayesian Factor close to zero (strong significance) for Rev, Comp and AC. However, a significant change was observed for the analysis based on AS grouping, as shown in Table 11. In the post-hoc analysis, it was identified that there was a significant difference between 8.5 and 15 mm group, and the mean difference was not significant between the 15 and 21.5 mm combination. It was also discussed in detail that the mean differences are so close and the distinction between significance and not was marginal. This Bayesian approach has shown a significant difference between both combinations, indicated both by lower Bayesian Factor and significance. The observations from both approaches (frequentist and Bayesian) have shown that the observations made are robust and are valid to make definitive conclusions.

3.5. Three-way analysis of variance

In the previous one-way ANOVA test and analysis, a uniform variation and the impact of independent variables are assumed to be mutually exclusive. In other words, the impact of the shape of aggregates on the compressive strength would be uniform across the other three independent parameters (aggregate size, AC ratio and compaction). However, the impact of independent parameters may not be linear and that the intersection of the independent variables may also be significant. For example, the impact shape of aggregates has on the compressive strength may be affected by the aggregate size and aggregate-to-cement ratio as well. A four-way ANOVA is therefore employed to assess the collective impact of independent parameters on the three performance (dependent) variables.

Table 11. Bayesian independent *t*-test output for T.Poro, M.Poro and Com.S for groups based on aggregate size (AS).

	Mean difference	Pooled std. error difference	Bayes factor[a]	t	df	Sig.(2-tailed)
Between aggregate size 8.5 and 15						
T.Poro	−0.0138	0.00899	3.584	−1.541	322	0.124
M.Poro	−0.0026	0.0114	11.119	−0.232	322	0.817
Com.S	−2.1256	1.01088	1.327	−2.103	322	0.036
Between aggregate size 8.5 and 21.5						
T.Poro	−0.0217	0.00898	0.672	−2.415	322	0.016
M.Poro	0.0186	0.01185	3.439	1.568	322	0.118
Com.S	−4.1532	1.14592	0.021	−3.624	322	0
Between aggregate size 15 and 21.5						
T.Poro	−0.0078	0.00848	7.522	−0.923	322	0.356
M.Poro	0.0212	0.0123	2.668	1.726	322	0.085
Com.S	−2.0277	1.0237	1.689	−1.981	322	0.048

[a]Bayes factor: Null versus alternative hypothesis.

Table 12 shows results of multivariate tests for the independent variables and their intersections with the performance variables. From general observation, it could established that all four test indicators (Pillai's Trace: PT, Wilk's Lambda: WL, Hotelling's Trace: HT and Roy's Largest Root: RLR) have shown the existence of significant variations between the impact of independent parameters on the three dependent performance variables, so a statistical significant above 99.9%. In addition, the intersection of the independent variables is also significant (all combinations) as indicated by a statistical significance above 99.9%. This establishes the fact that the impact of an independent parameter on all three dependent performance variables is non-linearly affected by variations in the other three independent variables. Considering the independent variables alone, it could be observed that the shape of aggregates (Rev) yields a higher F score on all 4 test indicators. For example, PT, WL, HT and RLR indicators have an F value of 809.3, 1213.4, 1790.1 and 3182.5, respectively for Revolutions. Simultaneously, the same indicator values are 117.6, 200.0, 309.1 and 603.8, respectively for AS (aggregate size). All four indicators show 5–7 times the F value of AS for Rev (Rev is higher), which indicates that the impact Rev imparts on the performance variables is 5–7 times that AS imparts on the same. On the contrary, all four test indicators have highly variable F value comparisons for both AC ratio and compaction. For example, the F value of PT for AC ratio shows a value comparable to AS (7 times lower than Rev) while the WL F value was 3 times more than AS (and almost 2 times lower than Rev). Contrastingly, HT- and RLR-F values are 2220.7 and 4463.2, respectively for AC, which was almost much higher (approximately 1.5 times) for Rev and corresponding values. Similar contrasting observations could also be observed for compaction, where PT-, WL-, HT- and RLR-F values are 138.0, 1066.4, 5152.8 and 10353.3 for Comp, which was 0.17, 0.88, 2.88 and 3.25 times the Rev values, respectively. PT is based on variances alone, but the advantage is that it is robust to assumption violations such as homogeneity and normal distributions while Wilk's Lambda is more sensitive to violations and sample sizes. While HT is also rather sensitive to sample inequalities, it does measure the group differences more accurately. RLR also assess the strongest difference more accurately and hence, for further discussions HT and RLR values are considered. It could be concluded that, while compaction had the highest impact on the performance variables, AS had the lowest impact on the performance parameters.

Looking at the F values of the intersections of independent design parameters, it could be observed that their impact is rather lower compared to individual independent variable F values, they have a significant impact on the performance variables. For example, the intersection of Rev∗AS has 172.3 and 326.6 for HT and RLR, respectively. This indicates that the impact Rev and AS impart together on the performance variables is less than the impact of AS on the same. All other binary intersections have a rather lower impact on the performance parameters with AC∗Comp yields the second highest

Table 12. Multivariate test results for all four independent parameters and their intersections.

Multivariate tests											
Effect		Value	F	Sig.	Partial Eta squared	Effect		Value	F	Sig.	Partial Eta squared
Intercept	Pillai's Trace	1.00	257409.5	0.000	0.999	AS * AC	Pillai's Trace	0.60	25.5	0.000	0.201
	Wilks' Lambda	0.00	257409.5	0.000	0.999		Wilks' Lambda	0.49	27.4	0.000	0.211
	Hotelling's Trace	1916.20	257409.5	0.000	0.999		Hotelling's Trace	0.85	28.5	0.000	0.221
	Roy's Largest Root	1916.20	257409.5	0.000	0.999		Roy's Largest Root	0.58	59.1	0.000	0.369
Rev	Pillai's Trace	1.71	809.3	0.000	0.857	AS * Comp	Pillai's Trace	0.72	31.7	0.000	0.238
	Wilks' Lambda	0.01	1213.4	0.000	0.900		Wilks' Lambda	0.36	42.2	0.000	0.290
	Hotelling's Trace	26.72	1790.1	0.000	0.930		Hotelling's Trace	1.60	53.5	0.000	0.348
	Roy's Largest Root	23.63	3182.5	0.000	0.959		Roy's Largest Root	1.47	149.0	0.000	0.595
AS	Pillai's Trace	0.93	117.6	0.000	0.466	AC * Comp	Pillai's Trace	0.78	35.7	0.000	0.260
	Wilks' Lambda	0.16	200.0	0.000	0.598		Wilks' Lambda	0.29	52.7	0.000	0.337
	Hotelling's Trace	4.61	309.1	0.000	0.698		Hotelling's Trace	2.18	73.0	0.000	0.421
	Roy's Largest Root	4.48	603.8	0.000	0.818		Roy's Largest Root	2.06	208.6	0.000	0.673
AC	Pillai's Trace	0.97	127.3	0.000	0.486	Rev * AS * AC	Pillai's Trace	1.45	47.7	0.000	0.485
	Wilks' Lambda	0.03	651.1	0.000	0.829		Wilks' Lambda	0.12	53.6	0.000	0.512
	Hotelling's Trace	33.14	2220.7	0.000	0.943		Hotelling's Trace	3.53	59.1	0.000	0.541
	Roy's Largest Root	33.14	4463.2	0.000	0.971		Roy's Largest Root	2.27	115.0	0.000	0.694
Comp	Pillai's Trace	1.01	138.0	0.000	0.506	Rev * AS * Comp	Pillai's Trace	0.86	20.2	0.000	0.285
	Wilks' Lambda	0.01	1066.4	0.000	0.888		Wilks' Lambda	0.34	21.7	0.000	0.300
	Hotelling's Trace	76.91	5152.8	0.000	0.975		Hotelling's Trace	1.38	23.0	0.000	0.314
	Roy's Largest Root	76.88	10353.3	0.000	0.987		Roy's Largest Root	0.87	44.0	0.000	0.465
Rev * AS	Pillai's Trace	1.53	105.9	0.000	0.511	Rev * AC * Comp	Pillai's Trace	0.49	9.8	0.000	0.163
	Wilks' Lambda	0.07	148.6	0.000	0.580		Wilks' Lambda	0.58	10.1	0.000	0.166
	Hotelling's Trace	5.15	172.3	0.000	0.632		Hotelling's Trace	0.61	10.2	0.000	0.169
	Roy's Largest Root	3.23	326.6	0.000	0.763		Roy's Largest Root	0.34	17.320	0.000	0.255
Rev * AC	Pillai's Trace	1.43	91.7	0.000	0.475	AS * AC * Comp	Pillai's Trace	0.83	19.5	0.000	0.278
	Wilks' Lambda	0.08	145.6	0.000	0.575		Wilks' Lambda	0.36	20.7	0.000	0.290
	Hotelling's Trace	6.04	202.2	0.000	0.668		Hotelling's Trace	1.30	21.8	0.000	0.302
	Roy's Largest Root	4.97	503.7	0.000	0.833		Roy's Largest Root	0.80	40.3	0.000	0.443
Rev * Comp	Pillai's Trace	0.88	41.8	0.000	0.292	Rev * AS * AC * Comp	Pillai's Trace	1.16	15.9	0.000	0.386
	Wilks' Lambda	0.33	46.8	0.000	0.311		Wilks' Lambda	0.22	16.8	0.000	0.399
	Hotelling's Trace	1.49	49.9	0.000	0.332		Hotelling's Trace	2.10	17.6	0.000	0.412
	Roy's Largest Root	1.03	104.8	0.000	0.509		Roy's Largest Root	1.21	30.6	0.000	0.547

Table 13. Test of between-subject effects for T.Poro, M.Poro and Com.S and the four independent variables and their intersections.

Tests of between-subjects effects							
Source		Type III sum of squares	df	Mean square	F	Sig.	Partial Eta squared
Corrected Model	T.Poro	3.1	80	0.04	562.6	0.000	0.991
	M.Poro	5.4	80	0.07	201.0	0.000	0.975
	Com.S	44718.0	80	558.97	284.1	0.000	0.982
Intercept	T.Poro	39.3	1	39.30	579130.4	0.000	0.999
	M.Poro	12.5	1	12.51	37205.4	0.000	0.989
	Com.S	114701.1	1	114701.11	58299.8	0.000	0.993
Rev	T.Poro	0.1	2	0.06	882.4	0.000	0.813
	M.Poro	2.4	2	1.19	3538.9	0.000	0.946
	Com.S	8229.9	2	4114.97	2091.5	0.000	0.912
AS	T.Poro	0.0	2	0.02	287.7	0.000	0.587
	M.Poro	0.0	2	0.02	64.5	0.000	0.242
	Com.S	1397.4	2	698.72	355.1	0.000	0.637
AC	T.Poro	0.7	2	0.35	5095.9	0.000	0.962
	M.Poro	0.2	2	0.12	369.6	0.000	0.646
	Com.S	12377.4	2	6188.70	3145.6	0.000	0.940
Comp	T.Poro	1.9	2	0.97	14243.6	0.000	0.986
	M.Poro	2.1	2	1.03	3065.1	0.000	0.938
	Com.S	13419.1	2	6709.53	3410.3	0.000	0.944
Rev * AS	T.Poro	0.1	4	0.01	190.4	0.000	0.653
	M.Poro	0.0	4	0.01	15.4	0.000	0.132
	Com.S	2435.3	4	608.83	309.5	0.000	0.753
Rev * AC	T.Poro	0.1	4	0.01	217.0	0.000	0.682
	M.Poro	0.2	4	0.04	130.7	0.000	0.564
	Com.S	2016.2	4	504.04	256.2	0.000	0.717
Rev * Comp	T.Poro	0.0	4	0.00	57.5	0.000	0.362
	M.Poro	0.1	4	0.01	43.3	0.000	0.300
	Com.S	295.1	4	73.78	37.5	0.000	0.270
AS * AC	T.Poro	0.0	4	0.00	31.9	0.000	0.240
	M.Poro	0.0	4	0.01	23.8	0.000	0.190
	Com.S	199.6	4	49.91	25.4	0.000	0.200
AS * Comp	T.Poro	0.0	4	0.00	34.9	0.000	0.256
	M.Poro	0.0	4	0.00	7.4	0.000	0.068
	Com.S	1045.7	4	261.42	132.9	0.000	0.568
AC * Comp	T.Poro	0.0	4	0.01	83.3	0.000	0.451
	M.Poro	0.0	4	0.01	27.5	0.000	0.214
	Com.S	1370.5	4	342.62	174.1	0.000	0.632
Rev * AS * AC	T.Poro	0.1	8	0.01	107.1	0.000	0.679
	M.Poro	0.1	8	0.01	39.0	0.000	0.435
	Com.S	447.6	8	55.95	28.4	0.000	0.360
Rev * AS * Comp	T.Poro	0.0	8	0.00	18.2	0.000	0.265
	M.Poro	0.0	8	0.00	14.8	0.000	0.227
	Com.S	451.9	8	56.49	28.7	0.000	0.362
Rev * AC * Comp	T.Poro	0.0	8	0.00	15.2	0.000	0.231
	M.Poro	0.0	8	0.00	6.9	0.000	0.120
	Com.S	170.7	8	21.34	10.8	0.000	0.176
AS * AC * Comp	T.Poro	0.0	8	0.00	21.2	0.000	0.295
	M.Poro	0.0	8	0.00	12.1	0.000	0.193
	Com.S	466.5	8	58.31	29.6	0.000	0.369
Rev * AS * AC * Comp	T.Poro	0.0	16	0.00	14.7	0.000	0.367
	M.Poro	0.1	16	0.01	26.8	0.000	0.514
	Com.S	394.9	16	24.68	12.5	0.000	0.331
Error	T.Poro	0.0	405	0.00			
	M.Poro	0.1	405	0.00			
	Com.S	796.8	405	1.97			
Total	T.Poro	42.4	486				
	M.Poro	18.0	486				
	Com.S	160215.9	486				
Corrected Total	T.Poro	3.1	485				
	M.Poro	5.5	485				
	Com.S	45514.8	485				

(73.0 and 208.6 for HT and RLR respectively). All other multitudes of 3 and 4 independent variable intersections yielded significantly lower impact on the performance variables.

While the above discussion established a significant impact of all four independent parameters on the three dependent performance variables, it does not provide details of the independent parameters and their intersections on each performance variable. Table 13 shows the detailed results of the impact independent variables and their intersections have on each dependent (performance) variable. Partial Eta Squared (PES) indicates how much percentage of the variance in the dependent variable is explained by each dependent corresponding variable. For example, Rev has a PES value of 0.813 for T.Poro, which could be interpreted as 81.3% of the variance in T.Poro could be explained by Rev (aggregate shape). Simultaneously, it could be observed that much higher (94.6% and 91.2%) of the variance in M.Poro and Com.S is attributed to Rev. While the variance attribution to AS is significantly reduced, it is lowest (24.2%) for M.Poro, indicating, aggregate size has much lower impact on M.Poro compared to T.Poro (58.7% and 63.7%). AC ratio on the other hand could be attributed to 96.2% and 94.0% for T.Poro and Com.S variances while only 64.6% could be attributed to M.Poro variance. This indicates that the impact the AC ratio has on M.Poro is much less compared to that it has on T.Poro and Com.S. Compaction has a high impact on all three performance variances indicated by more than 94–98%% attribution to variances.

If 81.3% of the variance in T.Poro is explained by Rev, the contribution of other parameters adds up to more than 100% attribution to T.Poro variances. This indicates that the intersections could also be significant. For example, the intersection Rev∗AS explains 65.3%, 13.2% and 75.3% of the variance in T.Poro, M.Poro and Com.S. While a significant contribution could be observed for T.Poro and Com.S from Rev∗AS intersection, much lower impact is observed on M.Poro. In other words, the impact Rev has on M.Poro is only slightly affected by the AS variation. The intersection Rev∗AC has moderate (56.4%–71.7%) on all three performance variables, most other intersections yield much lower contribution. Simultaneously, 3 and 4 independent variable intersections yield significantly lower, yet significant impacts on all three performance variables.

4. Conclusions

This study analyses the impact of aggregate size and shape on the porosities and compressive strength of pervious concrete, using a statistical assessment. The following conclusions are made:

(1) The shape of the aggregates influences the connectivity of pores as the gradient of Measured Porosity over Theoretical Porosity reduces with the increasing of the milling. Distribution analysis concludes that the impact of the shape of aggregate is minimal on Theoretical Porosity while significant in measured porosity and compressive strength.
(2) Milling the aggregates increases the uncertainty to predict the compressive strength by theoretical porosity or measured porosity. It concludes the influence of the other design parameters in the model.
(3) Even though the plots show that aggregate sizes have an impact on all three parameters, the one-way ANOVA and Post-HOC-LSD test confirm that measured porosity doesn't have a significance difference with any group, but theoretical porosity and compressive strength have a significant difference between 8.5 mm and 21.5 mm aggregate samples.
(4) The compaction energy impacts all three performance parameters significantly and the difference between the uncompacted and compacted samples is high.
(5) Providing optimum binder content will provide the proper packing of aggregate. The optimum A/C is between 3 and 4. The impact of A/C is higher than the shape of aggregate and lesser than compaction.
(6) A four-way ANOVA revealed that the intersections of independent parameters are significant with a reduced impact on the performance of pervious concrete. The results indicated that the shape of aggregates had the most substantial effect on compressive strength compared to

aggregate size, with F values for shape being 5–7 times higher than those for size. Compaction also showed a high impact, while aggregate size had the least influence on performance parameters. Intersections of independent variables, though impactful, were less significant than the individual variables. For example, the interaction of aggregate shape and size showed lower *F* values than aggregate shape alone.

(7) The analysis also included Partial Eta Squared (PES) values, showing that aggregate shape explained a substantial portion of the variance in all three performance variables, with particularly high values for total porosity. Conversely, aggregate size contributed less significantly to performance outcomes. The intersections of variables also demonstrated meaningful contributions to variance, particularly for total porosity, but generally had lower impacts than the main effects.

Disclosure statement

No potential conflict of interest was reported by the author(s).

Funding

This work was supported by the National Research Council of Sri Lanka: (Grant Number 19-045)

Data availability statement

The data are available for sharing, on request.

ORCID

Daniel Niruban Subramaniam http://orcid.org/0000-0002-1023-1617

References

Ahilash, N., Sajeevan, M., Subramaniam, D. N., & Rajakulendran, M. (2022). Optimising pervious concrete design with partial replacement of cement with fly ash. In *Proceedings road and airfield pavement technology* (pp. 495–505). Springer.

Akand, L., Yang, M., & Gao, Z. (2016). Characterization of pervious concrete through image based micromechanical modeling. *Construction and Building Materials*, *114*, 547–555. https://doi.org/10.1016/j.conbuildmat.2016.04.005

Anburuvel, A., & Subramaniam, D. N. (2022a). Investigation of the effects of compaction on compressive strength and porosity characteristics of pervious concrete. *Transportation Research Record: Journal of the Transportation Research Board*, *2676*(9), 513–525. https://doi.org/10.1177/03611981221087236

Anburuvel, A., & Subramaniam, D. N. (2023a). Effects of parameters on vertical porosity distribution in pervious concrete. *Magazine of Concrete Research*, *75*(7), 367–378. https://doi.org/10.1680/jmacr.21.00275

Anburuvel, A., & Subramaniam, D. N. (2023b). Influence of aggregate gradation and compaction on compressive strength and porosity characteristics of pervious concrete. *International Journal of Pavement Engineering*, *24*(2), 2055022. https://doi.org/10.1080/10298436.2022.2055022

Anburuvel, A., & Subramaniam, D. N. (2024). A novel multi-variable model for the estimation of compressive strength of pervious concrete. *International Journal of Pavement Research and Technology*, *17*(3), 720–731.

Andrew, I. N., & Bradley, J. P. (2010). Effect of aggregate size and gradation on pervious concrete mixtures. *ACI Materials Journal*, *107*(6), 627–633.

Awed, A., Kassem, E., Masad, E., & Little, D. (2015). Method for predicting the laboratory compaction behavior of asphalt mixtures. *Journal of Materials in Civil Engineering*, *27*(11), 04015016. https://doi.org/10.1061/(ASCE)MT.1943-5533.0001244

Bonicelli, A., Arguelles, G. M., & Pumarejo, L. G. F. (2016). Improving pervious concrete pavements for achieving more sustainable urban roads. *Procedia Engineering*, *161*, 1568–1573. https://doi.org/10.1016/j.proeng.2016.08.628

Bonicelli, A., Crispino, M., Giustozzi, F., & Shink, M. (2013). Laboratory analysis for investigating the impact of compaction on the properties of pervious concrete mixtures for road pavements. *Advanced Materials Research*, *723*, 409–419. https://doi.org/10.4028/www.scientific.net/AMR.723.409

Chandrappa, A. K., & Biligiri, K. P. (2018). Pore structure characterization of pervious concrete using x-ray microcomputed tomography. *Journal of Materials in Civil Engineering*, *30*(6), 04018108. https://doi.org/10.1061/(ASCE)MT.1943-5533.0002285

Chen, Y., Wang, K.-J., & Liang, D. (2012). Mechanical properties of pervious cement concrete. *Journal of Central South University*, *19*(11), 3329–3334. https://doi.org/10.1007/s11771-012-1411-9

Deo, O., Sumanasooriya, M., & Neithalath, N. (2010). Permeability reduction in pervious concretes due to clogging: Experiments and modeling. *Journal of Materials in Civil Engineering*, *22*(7), 741–751. https://doi.org/10.1061/(ASCE)MT.1943-5533.0000079

Haselbach, L. M., & Freeman, R. M. (2007). Effectively estimating in-situ porosity of pervious concrete from cores. *ASTM International*, *4*(7), 1–11.

Huang, B., Wu, H., Shu, X., & Burdette, E. G. (2010). Laboratory evaluation of permeability and strength of polymer-modified pervious concrete. *Construction and Building Materials*, *24*(5), 818–823. https://doi.org/10.1016/j.conbuildmat.2009.10.025

Huang, J., Zhang, Y., Sun, Y., Ren, J., Zhao, Z., & Zhang, J. (2021). Evaluation of pore size distribution and permeability reduction behavior in pervious concrete. *Construction and Building Materials*, *290*, 123228. https://doi.org/10.1016/j.conbuildmat.2021.123228

Jato-Espino, D., Rodriguez-Hernandez, J., Andrés-Valeri, V. C., & Ballester-Muñoz, F. (2014). A fuzzy stochastic multi-criteria model for the selection of urban pervious pavements. *Expert Systems with Applications*, *41*(15), 6807–6817. https://doi.org/10.1016/j.eswa.2014.05.008

Kirkham, R. H. H., & Whiffin, A. C. (1951). The compaction of concrete slabs by surface vibration: First series of experiments. *Magazine of Concrete Research*, *3*(8), 79–91. https://doi.org/10.1680/macr.1951.3.8.79

Kokubu, K., Cabrera, J. G., & Ueno, A. (1996). Compaction properties of roller compacted concrete. *Cement and Concrete Composites*, *18*(2), 109–117. https://doi.org/10.1016/0958-9465(95)00007-0

Kovac, M., & Sicakova, A. (2017). Changes of strength characteristics of pervious concrete due to variations in water to cement ratio. *IOP Conference Series: Earth and Environmental Science*, *92*, 012029. https://doi.org/10.1088/1755-1315/92/1/012029

Lian, C., & Zhuge, Y. (2010). Optimum mix design of enhanced permeable concrete – an experimental investigation. *Construction and Building Materials*, *24*(12), 2664–2671. https://doi.org/10.1016/j.conbuildmat.2010.04.057

Mueller, F. V., Wallevik, O. H., & Khayat, K. H. (2014). Linking solid particle packing of Eco-SCC to material performance. *Cement and Concrete Composites*, *54*, 117–125. https://doi.org/10.1016/j.cemconcomp.2014.04.001

Neithalath, N., Sumanasooriya, M. S., & Deo, O. (2010). Characterizing pore volume, sizes, and connectivity in pervious concretes for permeability prediction. *Materials Characterization*, *61*(8), 802–813. https://doi.org/10.1016/j.matchar.2010.05.004

Nguyen, D. H., Sebaibi, N., Boutouil, M., Leleyter, L., & Baraud, F. (2014). A modified method for the design of pervious concrete mix. *Construction and Building Materials*, *73*, 271–282. https://doi.org/10.1016/j.conbuildmat.2014.09.088

Obla, K. H. (2007). Pervious concrete for sustainable development. *Recent Advances in Concrete Technology*, *September*, 151–174.

Pieralisi, R., Cavalaro, S. H. P., & Aguado, A. (2015). Evolutionary lattice model for the compaction of pervious concrete in the fresh state. *Construction and Building Materials*, *99*, 11–25. https://doi.org/10.1016/j.conbuildmat.2015.08.143

Pieralisi, R., Cavalaro, S. H. P., & Aguado, A. (2016). Discrete element modelling of the fresh state behavior of pervious concrete. *Cement and Concrete Research*, *90*, 6–18. https://doi.org/10.1016/j.cemconres.2016.09.010

Pietzsch, D., & Poppy, W. (1992). Simulation of soil compaction with vibratory rollers. *Journal of Terramechanics*, *29*(6), 585–597. https://doi.org/10.1016/0022-4898(92)90038-L

Reyad, M., ElTair, A. M., El-Nemr, A., & Jato-Espino, D. (2024). Mechanical and permeability behavior of porous concrete when using different aggregate sizes and adding polypropylene fiber. *Journal of Materials in Civil Engineering*, *36*(6), 04024132. https://doi.org/10.1061/JMCEE7.MTENG-16429

Sajeevan, M., & Subramaniam, D. N. (2023). Investigation of boundary layer impact on pervious concrete. *International Journal of Pavement Engineering*, *24*(2), 2111423. https://doi.org/10.1080/10298436.2022.2111423

Sajeevan, M., Subramaniam, D. N., Rinduja, R., & Pratheeba, J. (2023). Investigation of compaction on compressive strength and porosity of pervious concrete. *International Journal of Pavement Research and Technology*. https://doi.org/10.1007/s42947-023-00377-w.

Sandoval, G. F. B., Galobardes, I., Campos, A., & Toralles, B. M. (2020). Assessing the phenomenon of clogging of pervious concrete (Pc): Experimental test and model proposition. *Journal of Building Engineering*, *29*, 101203. https://doi.org/10.1016/j.jobe.2020.101203

Sathiparan, N., Jeyananthan, P., & Subramaniam, D. N. (2024a). Effect of aggregate size, aggregate to cement ratio and compaction energy on ultrasonic pulse velocity of pervious concrete: Prediction by an analytical model and machine learning techniques. *Asian Journal of Civil Engineering*, *25*(1), 495–509. https://doi.org/10.1007/s42107-023-00790-3

Sathiparan, N., Jeyananthan, P., & Subramaniam, D. N. (2024b). Surface response regression and machine learning techniques to predict the characteristics of pervious concrete using non-destructive measurement: Ultrasonic pulse velocity and electrical resistivity. *Measurement*, *225*, 114006. https://doi.org/10.1016/j.measurement.2023.114006

Shen, P., Lu, J.-X., Zheng, H., Liu, S., & Sun Poon, C. (2021). Conceptual design and performance evaluation of high strength pervious concrete. *Construction and Building Materials*, *269*, 121342. https://doi.org/10.1016/j.conbuildmat.2020.121342

Shu, X., Huang, B., Wu, H., Dong, Q., & Burdette, E. G. (2011). Performance comparison of laboratory and field produced pervious concrete mixtures. *Construction and Building Materials*, *25*(8), 3187–3192. https://doi.org/10.1016/j.conbuildmat.2011.03.002

Singh, A., Jagadeesh, G. S., Sampath, P. V., & Biligiri, K. P. (2019). Rational approach for characterizing *in situ* infiltration parameters of two-layered pervious concrete pavement systems. *Journal of Materials in Civil Engineering*, *31*(11), 04019258. https://doi.org/10.1061/(ASCE)MT.1943-5533.0002898

Sonebi, M., & Bassuoni, M. T. (2013). Investigating the effect of mixture design parameters on pervious concrete by statistical modelling. *Construction and Building Materials*, *38*, 147–154. https://doi.org/10.1016/j.conbuildmat.2012.07.044

Sriravindrarajah, R., Wang, N. D. H., & Ervin, L. J. W. (2012). Mix design for pervious recycled aggregate concrete. *International Journal of Concrete Structures and Materials*, *6*(4), 239–246. https://doi.org/10.1007/s40069-012-0024-x

Subramaniam, D. N., Dassanayake, D. H. H. P., Ahilash, N., Wijekoon, S. H. B., & Sathiparan, N. (2024a). Characterisation of the shape of aggregates using image analysis. *International Journal of Pavement Engineering*, *25*(1), 2349905. https://doi.org/10.1080/10298436.2024.2349905

Subramaniam, D. N., Hareindirasarma, S., & Janarthanan, B. (2022). An alternative approach to optimize aggregate-to-cement ratio and compaction in pervious concrete. *Arabian Journal for Science and Engineering*, *47*(10), 13063–13071. https://doi.org/10.1007/s13369-022-06737-1

Subramaniam, D. N., Jeyananthan, P., & Sathiparan, N. (2024b). Soft computing techniques to predict the electrical resistivity of pervious concrete. *Asian Journal of Civil Engineering*, *25*(1), 711–722. https://doi.org/10.1007/s42107-023-00806-y

Subramaniam, D. N., Sajeevan, M., Pratheeba, J., Wijekoon, S. H. B., & Sathiparan, N. (2024). Characterization of the shape of aggregates using image analysis and machine learning classification tools. *Geomechanics and Geoengineering*, *19*(4), 421–443. https://doi.org/10.1080/17486025.2023.2288655

Supriya, A., & Murali, K. (2023). The development of the compressive strength of pervious concrete using sugarcane bagasse ash and flyash. *Materials Today: Proceedings*. https://doi.org/10.1016/j.matpr.2023.04.338.

Tang, B., Fan, M., Yang, Z., Sun, Y., & Yuan, L. (2023). A comparison study of aggregate carbonation and concrete carbonation for the enhancement of recycled aggregate pervious concrete. *Construction and Building Materials*, *371*, 130797. https://doi.org/10.1016/j.conbuildmat.2023.130797

Torres, A., Hu, J., & Ramos, A. (2015). The effect of the cementitious paste thickness on the performance of pervious concrete. *Construction and Building Materials*, *95*, 850–859. https://doi.org/10.1016/j.conbuildmat.2015.07.187

Wang, Z., Zou, D., Liu, T., Zhou, A., & Shen, M. (2020). A novel method to predict the mesostructure and performance of pervious concrete. *Construction and Building Materials*, *263*, 120117. https://doi.org/10.1016/j.conbuildmat.2020.120117

Wen, F., Fan, H., Zhai, S., Zhang, K., & Liu, F. (2020). Pore characteristics analysis and numerical seepage simulation of antifreeze permeable concrete. *Construction and Building Materials*, *255*, 119310. https://doi.org/10.1016/j.conbuildmat.2020.119310

Wijekoon, S. H. B., Sathiparan, N., & Subramaniam, D. N. (2024b). Optimisation of pervious concrete performance by varying aggregate shape, size, aggregate-to-cement ratio, and compaction effort by using the Taguchi method. *International Journal of Pavement Engineering*, *25*(1), 2380523. https://doi.org/10.1080/10298436.2024.2380523

Wijekoon, S. H., Shajeefpiranath, T., Subramaniam, D. N., & Sathiparan, N. (2024a). A mathematical model to predict the porosity and compressive strength of pervious concrete based on the aggregate size, aggregate-to-cement ratio and compaction effort. *Asian Journal of Civil Engineering*, *25*(1), 67–79. https://doi.org/10.1007/s42107-023-00757-4

Wijekoon, S. H. B., Subramaniam, D. N., & Sathiparan, N. (2023). Statistical assessment of different aggregate shape factors. *International Journal of Pavement Research and Technology*. https://doi.org/10.1007/s42947-023-00398-5.

Xie, X., Zhang, T., Yang, Y., Lin, Z., Wei, J., & Yu, Q. (2018). Maximum paste coating thickness without voids clogging of pervious concrete and its relationship to the rheological properties of cement paste. *Construction and Building Materials*, *168*, 732–746. https://doi.org/10.1016/j.conbuildmat.2018.02.128

Xu, G., Shen, W., Fang, D., Zhou, M., Zhang, B., Du, X., & Zhang, D. (2020). Influence of size and surface condition of distributing-filling coarse aggregate on the properties of aggregate-interlocking concrete. *Construction and Building Materials*, *261*, 120002. https://doi.org/10.1016/j.conbuildmat.2020.120002

Yu, F., Guo, J., Liu, J., Cai, H., & Huang, Y. (2023). A review of the pore structure of pervious concrete: Analyzing method, characterization parameters and the effect on performance. *Construction and Building Materials*, *365*, 129971. https://doi.org/10.1016/j.conbuildmat.2022.129971

Zhang, C., Wang, H., You, Z., & Yang, X. (2016). Compaction characteristics of asphalt mixture with different gradation type through superpave gyratory compaction and x-ray CT scanning. *Construction and Building Materials*, *129*, 243–255. https://doi.org/10.1016/j.conbuildmat.2016.10.098

Zhong, R., & Wille, K. (2015). Material design and characterization of high performance pervious concrete. *Construction and Building Materials*, *98*, 51–60. https://doi.org/10.1016/j.conbuildmat.2015.08.027

Zhu, Y., Fu, H., Wang, P., Xu, P., Ling, Z., & Wei, D. (2023). Pore structure characteristics, mechanical properties, and freeze–thaw resistance of vegetation-pervious concrete with unsintered sludge pellets. *Construction and Building Materials*, *382*, 131342. https://doi.org/10.1016/j.conbuildmat.2023.131342